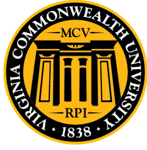

Virginia Commonwealth University
VCU Scholars Compass

Theses and Dissertations Graduate School

2005

STM Studies of Oxygen Etching of Silicon Surfaces

Mary L. Willis
Virginia Commonwealth University

Follow this and additional works at: https://scholarscompass.vcu.edu/etd

Part of the Physics Commons

© The Author

Downloaded from
https://scholarscompass.vcu.edu/etd/1008

This Thesis is brought to you for free and open access by the Graduate School at VCU Scholars Compass. It has been accepted for inclusion in Theses and Dissertations by an authorized administrator of VCU Scholars Compass. For more information, please contact libcompass@vcu.edu.

المنارة للاستشارات

www.manaraa.com

AFM Studies of Oxygen Etching of Silicon Surfaces

A thesis submitted in partial fulfillment of the requirements for the degree of Master of Science in Physics / Applied Physics at Virginia Commonwealth University.

By

Mary L. Willis

B.S. in Physics

Macalester College, 1982

M.S. in Physics/Applied Physics

Virginia Commonwealth University, 2005

Director: Alison A. Baski, Associate Professor, Department of Physics

Virginia Commonwealth University,

Richmond, Virginia, 23284

August 2005

Acknowledgments

As with any endeavor, there are many people who deserve credit for this work. Everyone in the Physics Department has played a role in my work.

Thanks go to Dr. Alison Baski for allowing me to work in her lab and the assistance she gave me in understanding surface science. Thanks also go to Karle Cooper and John Skrobiszewski in teaching me to use the AFM. John Skrobiszewski also helped image and prepare some of the surfaces presented in this paper. Special thanks go to Jon Dickinson for all his support and teaching my first year in the lab.

Lastly, I could not have done this without the love and support of my family. Aoky and Wolf spent many happy hours in the lab; their patience and understanding meant so much to me. The boys have gained an enduring love of Physics from this experience.

This work was partially supported by the National Science Foundation.

Table of Contents

Acknowledgments ii

List of Figures iv

Abstract vi

Chapter 1: Introduction 1

1.1 Experimental Details 1

1.2 Atomic Force Microscopy (AFM) 2

1.3 Oxygen Etching of Silicon 3

1.4 Chapter 1 Figures 5

Chapter 2: Etching of Stable Si(001), Si(111), and Si(113) Surfaces 8

2.1 O_2 Etching of Si(001) 8

2.2 O_2 Etching of Si(111) 9

2.3 O_2 Etching of Si(113) 10

2.4 Chapter 2 Figures 11

Chapter 3: Oxygen Etching of Unstable Si(5 5 12) and Si(112) Surfaces 18

3.1 O_2 Etching of Si(5 5 12) 18

3.2 O_2 Etching of Si(112) 19

3.3 Chapter 3 Figures 21

References 31

Appendix 33

List of Figures

Fig. 1.1: Schematic of atomic force microscopy. 5

Fig. 1.2: Schematic showing two possible reactions of O_2 incident on a Si surface 6

Fig. 1.3: Stable silicon orientations in the (001) to (111) family of surfaces, with "thumbnail" STM images of each surface reconstruction 7

Fig. 2.1: Schematic of silicon orientations with those surfaces stable to oxygen etching highlighted: Si(001), Si(113), and Si(111). 11

Fig. 2.2: AFM images (2×2 μm^2) of 200 L O_2/Si(001) as a function of temperature at (a–d) 3.3×10^{-7} Torr and (e–h) 1.5×10^{-7} Torr. 12

Fig. 2.3: AFM images (5×5 μm^2) of 200 L O_2/Si(001) as a function of temperature at (a–d) 3.3×10^{-7} Torr and (e–h) 1.5×10^{-7} Torr. 13

Fig. 2.4: AFM images (2×2 μm^2) of 200 L O_2/Si(111) as a function of temperature at (a–d) 3.3×10^{-7} Torr and (e–h) 1.5×10^{-7} Torr. 14

Fig. 2.5: AFM images (5×5 μm^2) of 200 L O_2/Si(111) as a function of temperature at (a–d) 3.3×10^{-7} Torr and (e–h) 1.5×10^{-7} Torr. 15

Fig. 2.6: AFM images (2×2 μm^2) of 200 L O_2/Si(113) as a function of temperature at (a–d) 3.3×10^{-7} Torr and (e–h) 1.5×10^{-7} Torr. 16

Fig. 2.7: AFM images (5×5 μm^2) of 200 L O_2/Si(113) as a function of temperature at (a–d) 3.3×10^{-7} Torr and (e–h) 1.5×10^{-7} Torr. 17

Fig. 3.1: Schematic of Si orientations with those surfaces unstable to oxygen etching highlighted: Si(112) and Si(5 5 12). 21

Fig. 3.2: AFM images (2×2 μm^2) of 200 L O_2/Si(5 5 12) as a function of temperature at (a-d) 3.3×10^{-7} Torr and (e-h) 1.5×10^{-7} Torr. 22

Fig. 3.3: AFM images (5×5 μm^2) of 200 L O_2/Si(5 5 12) as a function of temperature at (a-d) 3.3×10^{-7} Torr and (e-h) 1.5×10^{-7} Torr. 23

Fig. 3.4: Cross-section of "intermediate" sawtooth facets for O_2/Si(5 5 12) with 200 L at 800 °C. 24

Fig. 3.5: Cross-section of "final" sawtooth facets for O_2/Si(5 5 12) with 400 L at 800 °C. 25

Fig. 3.6: (a-e) 2×2 μm^2 and (f-j) 5×5 μm^2 AFM images of 200 L O_2/Si(112) as a function of temperature at 3.3×10^{-7} Torr. ... 26

Fig. 3.7: (a-d) 2×2 μm^2 and (e-h) 5×5 μm^2 AFM images of O_2/Si(112) as a function of oxygen exposure at 3.3×10^{-7} Torr and 800 °C. ... 27

Fig. 3.8: (a-e) 2×2 μm^2 and (f-j) 5×5 μm^2 AFM images of O_2/Si(112) system as a function of exposure at 3.3×10^{-7} Torr and 850 °C. ... 28

Fig. 3.9: Cross-section of “intermediate” sawtooth facets for O_2/Si(112) with 200 L at 800 °C. ... 29

Fig. 3.10: Cross-section of “final” sawtooth facets for O_2/Si(112) with 400 L at 850 °C. ... 30

Abstract

STM Studies of Oxygen Etching of Silicon Surfaces

By Mary L. Willis, M.S.

A thesis submitted in partial fulfillment of the requirements for the degree of Master of Science at Virginia Commonwealth University, 20053.

Major Director: Alison A. Baski, Associate Professor, Department of Physics

This study uses atomic force microscopy (AFM) to investigate the oxygen etching behavior of the following silicon surface orientations: (001), (111), (113), (5 5 12) and (112). Most etching was performed at sample temperatures between 650 °C and 800 °C, at pressures of 3.3×10^{-7} and 1.5×10^{-7} Torr, and at an exposure of 200 L. Surface orientation strongly influences the morphology resulting from extended etching. The surface orientations that are stable against etching and remain flat include Si(001), Si(111), and Si(113). Such surfaces also include island structures, which result from etching around oxide-induced pinning sites. The density of these islands increases at lower temperatures and higher pressures. The surface orientations that are unstable against oxygen etching and facet to other orientations include Si(5 5 12) and Si(112). These surfaces form sawtooth facets that are primarily composed of more stable (111) and (113) planes. By controlling the temperature and exposure during oxygen etching, it is therefore possible to form a variety of surface morphologies.

Chapter 1: Introduction

The interaction of oxygen with Si surfaces is of fundamental importance in Si-based semiconductor research and technology, since oxygen interactions with Si can degrade device performance. Much research has already gone into this area to study the process of silicon oxidation.[1,2] The basic chemical reaction is $Si + O_2 \rightarrow SiO_2$ for oxidation and $2Si + O_2 \rightarrow 2SiO$ for etching (see Fig. 1.2); however, the intermediate steps are not yet clearly understood.[3–12] Surface defects and step edges further complicate matters with their enhanced reactivity.[13] As the drive to create smaller devices continues, the need to understand and ultimately control the reaction of O_2 with Si surfaces remains an important issue.

Up to this point, most studies have concentrated on the low-index Si(001)[7,8,13,14–23] and Si(111)[2,10,24–34] surfaces. Such studies have primarily examined oxygen reactions at low exposures and temperatures using the technique of scanning tunneling microscopy (STM). In this work, we use the technique of atomic force microscopy (AFM) to study oxygen etching on a much larger variety of silicon orientations at higher exposures. The use of AFM instead of STM allows the efficient acquisition of large-scale surface morphology data.

1.1 Experimental Details

These experiments were carried out using commercially prepared silicon samples cut from wafers oriented to within 0.5° of the (001), (111), (112), (113), or (5 5 12) orientations (see Figure 1.3). The samples were prepared in an ion-pumped, ultra-high vacuum (UHV) system ($P < 5\times10^{-10}$ Torr). First, the native oxide layer on the Si sample was removed and a clean surface obtained. This was accomplished by preheating the sample holder to remove contaminants, then passing direct current through the Si sample to heat it to 1250 °C for ~10 s ($P < 1 \times 10^{-8}$ Torr). The temperature was measured by an

infrared pyrometer. The sample was then exposed to oxygen by leaking research grade O_2 (99.995%) into the main chamber from a back-filled mini-chamber (5×10^{-3} Torr), which had been previously pumped to 5×10^{-6} Torr. During O_2 exposure, the sample was held at temperatures between 650 and 800 °C and then exposed to 200 Langmuirs (L) (1 L is equivalent to 1 s exposure at 1×10^{-6} Torr). The pressures used in this study were chosen to be 3.3×10^{-7} Torr and 1.5×10^{-7} Torr, because they required reasonable exposure times and were sufficiently low that the UHV chamber pressure could recover after exposure. Once the exposure was complete, the sample current was immediately turned off to quench the sample. After cooling to room temperature, the Si samples were then removed from the UHV chamber and examined using atomic force microscopy (AFM). The samples presented in this study were prepared over a period of 18 months.

1.2 Atomic Force Microscopy (AFM)

The atomic force microscope is a scanning probe microscope based on the detection of forces between a tip and sample surface. This technique produces images of the sample surface topography ranging in size from 1×1 μm^2 to 100×100 μm^2. The tip is at the end of a micro-cantilever with a very small force constant (see Fig. 1.1). A laser focused on the back of the cantilever is used to track the vertical motion of the tip as it rasters across the surface. The laser reflects onto a two-sector photodiode that is part of a feedback circuit. This circuit adjusts the vertical height of the tip in order to maintain a constant force between the tip and sample. The tip height (or z-piezo voltage) is recorded during scanning to produce a topographic image of the surface. In this study, tapping™ mode was used in order to minimize sample damage and to obtain higher imaging resolution. In this mode, the tip vibrates at its resonant frequency and "taps" the surface, where the change in oscillation amplitude is monitored.

1.3 Oxygen Etching of Silicon

Exposure of a Si substrate to research-grade O_2 can produce oxide growth, etching or both, depending on the substrate temperature and oxygen pressure. At lower temperatures and higher exposures, oxidation dominates with oxygen and Si bonding to create SiO_2 (see Fig. 1.2). At higher temperatures and lower exposures, etching dominates with the formation of volatile SiO that desorbs from the surface.[35] Seiple and Pelz have proposed a phase diagram,[21] which indicates the pressure-temperature conditions necessary for etching vs. oxide growth. They do not propose a well-defined boundary between the etching and nucleation regimes, rather, a transition region exists where both processes occur. This transition region leads to interesting changes in the surface morphology and is the subject of this study.

Pressure and temperature are critical variables during oxygen etching because they determine the arrival rate of O_2 and how quickly it diffuses across the surface. The rate at which O_2 hits the surface is determined by pressure, where a higher pressure yields a higher O_2 arrival rate. The rate at which O_2 diffuses across the surface is determined by temperature, where a higher temperature leads to faster surface diffusion. If the pressure is high and the temperature is low, then the arrival rate of O_2 is fast compared to the diffusion rate. Diffusing atoms are more likely to encounter other atoms and nucleate an oxide region. If, on the other hand, the pressure is low and the temperature high, then the diffusion rate is high compared to the arrival rate. The diffusing atoms are more likely to form volatile SiO and etch the surface. In addition to the relative dominance of oxide growth vs. etching, pressure and temperature also determine where reactions occur. If diffusion lengths are large, then there is a higher probability that atoms will form oxide or etch at the more reactive step edges.

In this study, five Si surface orientations are examined (see Fig. 1.3). These orientations are classified as low-index, Si(001) and Si(111), and high-index, Si(113),

Si(5 5 12) and Si(112). Previous studies have shown that high-index Si surfaces such as Si(5 5 12) are unstable when exposed to metals (Gd, Au) and will preferentially form lower-energy planes such as Si(111) and Si(113).[36,37,38] We will see that this is also the case for oxygen etching of such a surface.[39]

1.4 Chapter 1 Figures

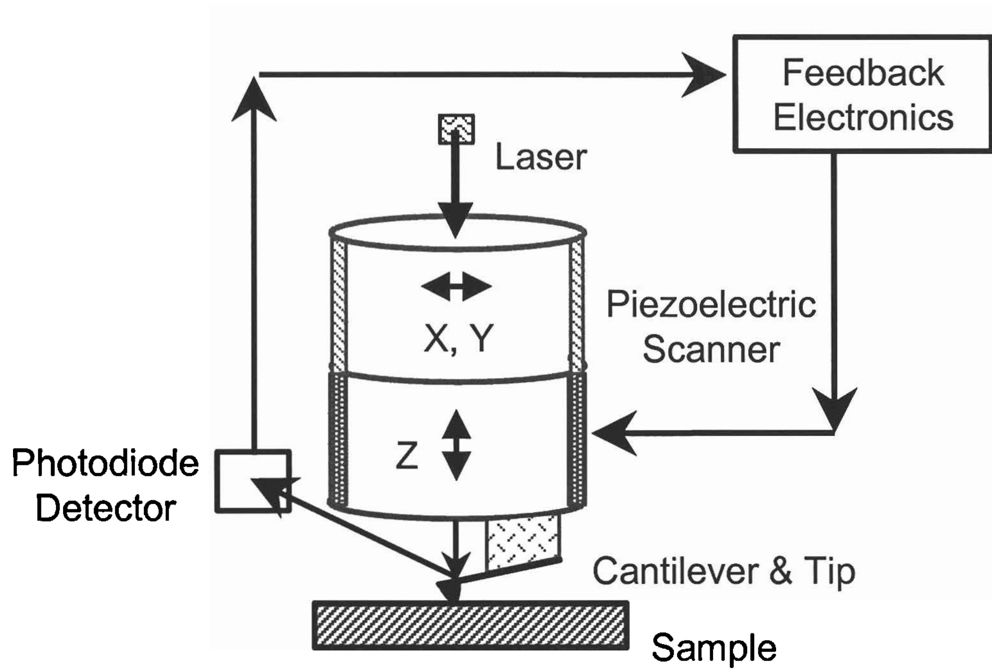

Fig. 1.1: Schematic of atomic force microscopy.

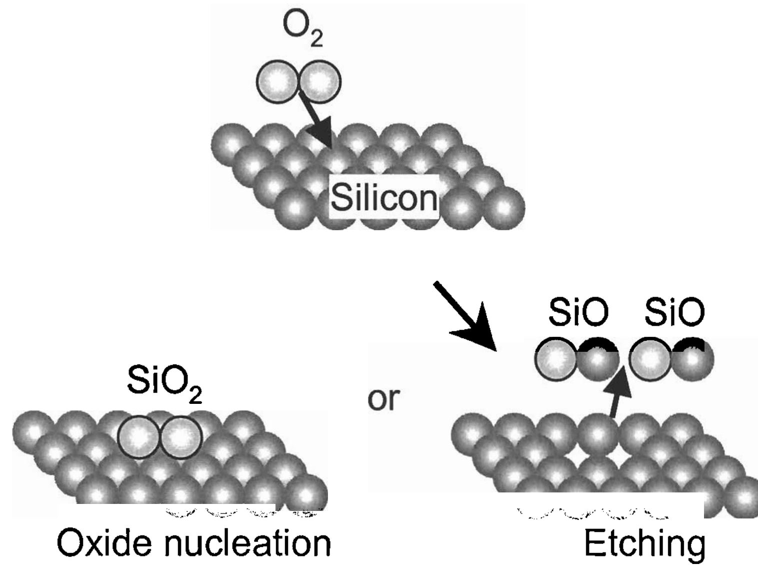

Fig. 1.2: Schematic showing two possible reactions of O_2 incident on a Si surface

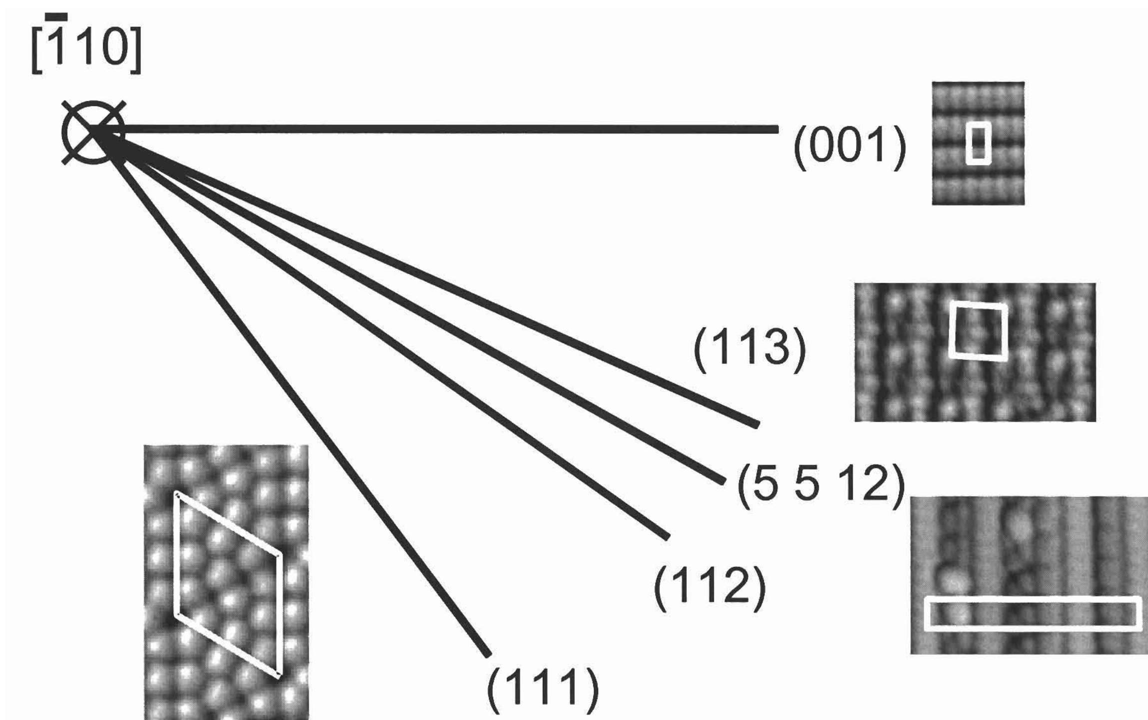

Fig. 1.3: Stable silicon orientations in the (001) to (111) family of surfaces, with "thumbnail" STM images of each surface reconstruction

Chapter 2: Etching of Stable Si(001), Si(111), and Si(113) Surfaces

Previous research has shown that at low exposure and temperature (50 L and 700 °C), most Si surface orientations appear similar after oxygen etching. However, at high exposure and temperature (200–400 L and 800 °C), the surfaces can have significantly different large-scale morphologies.[39] This study focuses on the surface morphologies that result from extended etching of five different Si orientations: (001), (111), (113), (5 5 12), and (112). The exposure is held constant at 200 L with a range of temperatures from 650 to 800 °C and pressures of 3.3×10^{-7} and 1.5×10^{-7} Torr. In this chapter, those surface orientations that remain stable after extended etching are discussed. These orientations include the low-index Si(001) and Si(111) surfaces, as well as the stable high-index Si(113) surface. All of these surfaces form islands during etching that result from oxide-induced pinning sites (see Fig. 2.1).

2.1 O_2 Etching of Si(001)

A summary of the temperature dependence for etching of Si(001) is shown in Figs. 2.2 and 2.3. In this study, oxygen exposure at the lowest sample temperature of 650 °C results in a uniform oxide layer (see Fig. 2.2a). Significant etching does not occur until ~700 °C, where islands are formed by etching around oxide-induced "pinning" sites. Such pinning sites prevent the desorption of Si in that region, resulting in islands that increase in height with increased etching time. The islands form uniformly across the surface, with their density decreasing as the temperature increases due to fewer pinning sites. For the higher pressure conditions (3.3×10^{-7} Torr), the island density ranges from 150 μm^{-2} at 700 °C to 13 μm^{-2} at 800 °C. For the lower pressure conditions (1.5×10^{-7} Torr), the density ranges from 139 μm^{-2} at 700 °C to 5 μm^{-2} at 800 °C. Notice that the island density on the higher pressure samples is larger at a given temperature than that on the lower pressure samples. This occurs because the arrival rate of oxygen molecules is

greater at higher pressures and results in a higher density of diffusing species on the surface. As a result, the oxygen species interact more frequently to nucleate a higher density of oxide-induced pinning sites.

The size of the islands appears to be uniform at a given pressure/temperature condition, but the island size increases for higher temperatures. This size effect is presumably because surface etching is more prevalent at higher temperatures and a larger oxide-induced pinning site is necessary to stabilize an island. Island diameters increase from 40 nm at 700 °C to 140 nm at 800 °C at higher pressures, and from 30 nm at 700 °C to 200 nm at 800 °C at lower pressures. The average height of the islands also increases with temperature, e.g. from ~1.5 nm at 700 °C to ~2 nm at 800 °C, consistent with the higher etching rate at higher temperatures. Finally, at higher temperatures the island shape becomes more well-defined with edges along the two-fold symmetry directions of the Si(001) surface.

2.2 O_2 Etching of Si(111)

In contrast to Si(001), the island morphology produced by etching of Si(111) noticeably changes as a function of temperature. At the lower temperatures of 650 °C and 700 °C, islands preferentially nucleate along step edges and domain boundaries, leading to an inhomogeneous island density (Fig. 2.4 a,b,e,f). At 750 °C and 800 °C, however, islands of similar size and shape homogeneously cover on the surface (Fig. 2.4 c,d,g,h). Although the island density is homogeneous, the islands preferentially occur along step edges, pinning the retraction of steps in their vicinity. In fact very few islands are found within the terraces, unlike at the lower temperatures. As expected, the island density decreases as temperature increases. Contrary to expectations, however, the island density at 800 °C for the high pressure data (Fig. 2.4a-d) is noticeably lower than that for the low pressure data (Fig. 2.4e-h). This may be due to a change in sample preparation conditions, since these samples were prepared four months apart. The average island

height increases with temperature from 1–2 nm at 750 °C to ~2 nm at 800 °C. With respect to island shape, at the higher temperatures the islands develop relatively well-defined edges along the three-fold symmetry directions of the (111) surface.

2.3 O_2 Etching of Si(113)

Etching of the Si(113) surface is more similar to that of Si(111) than Si(001). As shown in Figs. 2.6 and 2.7, there is inhomogeneous island nucleation at lower temperatures and a relatively uniform island density at higher temperatures. It should be noted that the surface morphologies for the two different pressure conditions shown in Fig. 2.6 do not appear as similar as for the (001) and (111) data. Unlike for the low-index surfaces, the Si(113) data has been taken from a variety of sample runs that extend over a period over six months. Regardless, as with the previous surfaces, the island density decreases and island size increases as the temperature increases. In the case of Si(113), however, the island shape is anisotropic at the higher temperatures. This behavior reflects the anisotropic nature of the underlying surface. Extended etching produces finger-like islands with straight edges along the $[\bar{1}10]$ direction, which is the row direction of the Si(113)3×2 surface reconstruction. Prior STM studies have shown that some of the well-defined edges correspond to short planes of the nearby (337) orientation. Although the island morphology on Si(113) at higher temperatures is not very similar to (001) or (111), the Si(113) surface remains planar under extended etching, just as is the case for the low-index surfaces.

2.4 Chapter 2 Figures

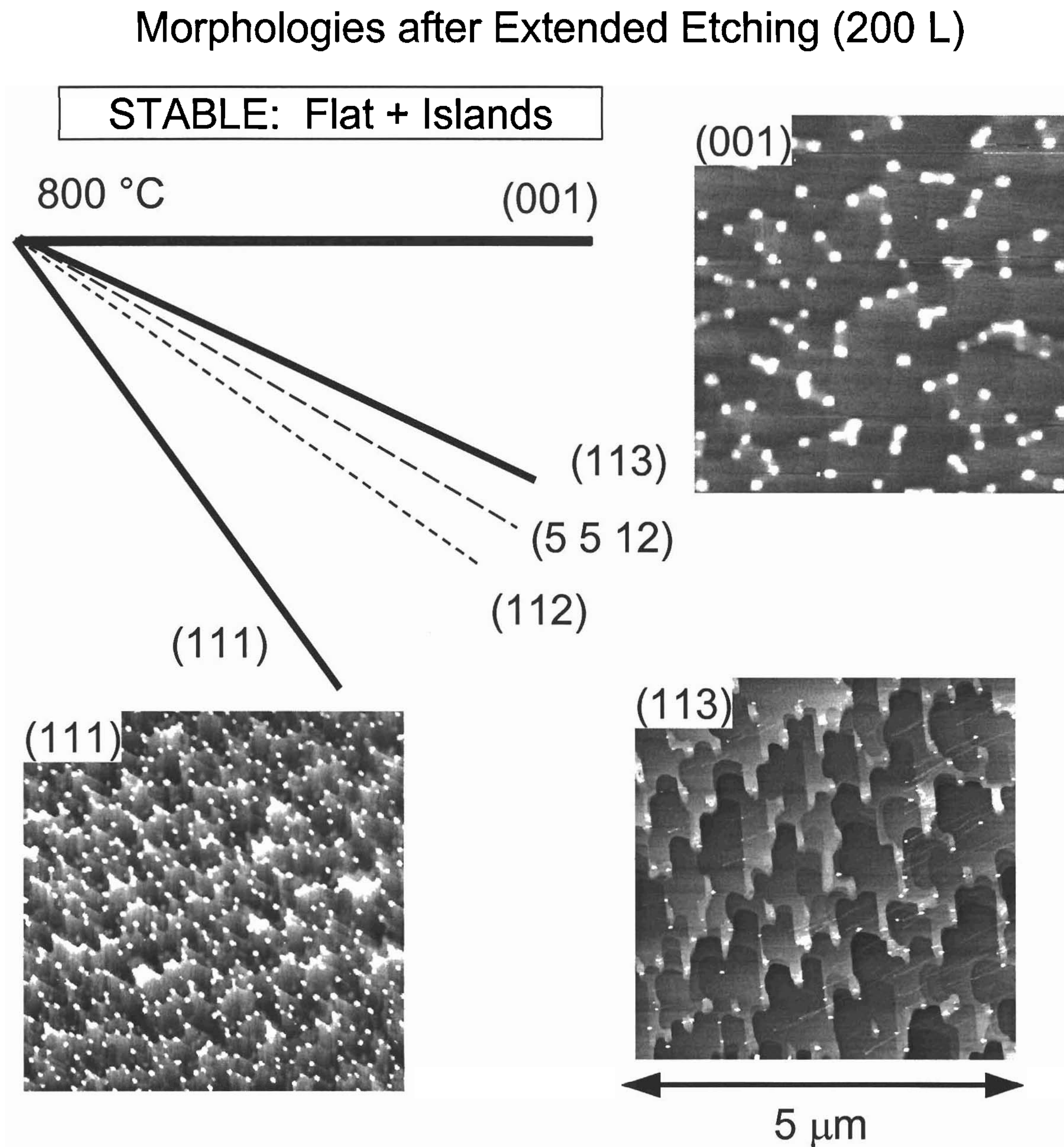

Fig. 2.1: Schematic of silicon orientations with those surfaces stable to oxygen etching highlighted: Si(001), Si(113), and Si(111).

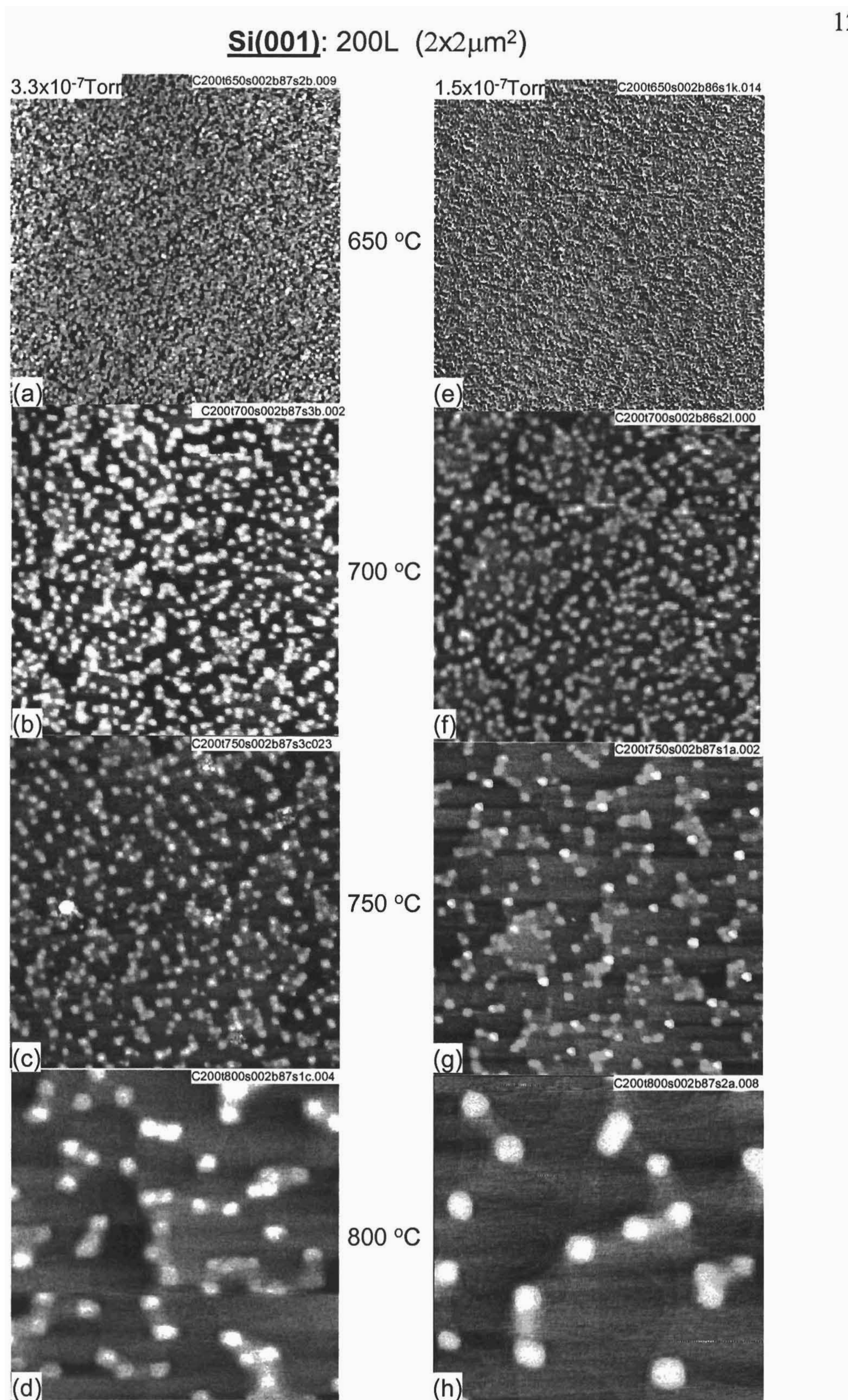

Fig. 2.2: AFM images (2×2 μm^2) of 200 L O_2/Si(001) as a function of temperature at (a–d) 3.3×10^{-7} Torr and (e–h) 1.5×10^{-7} Torr.

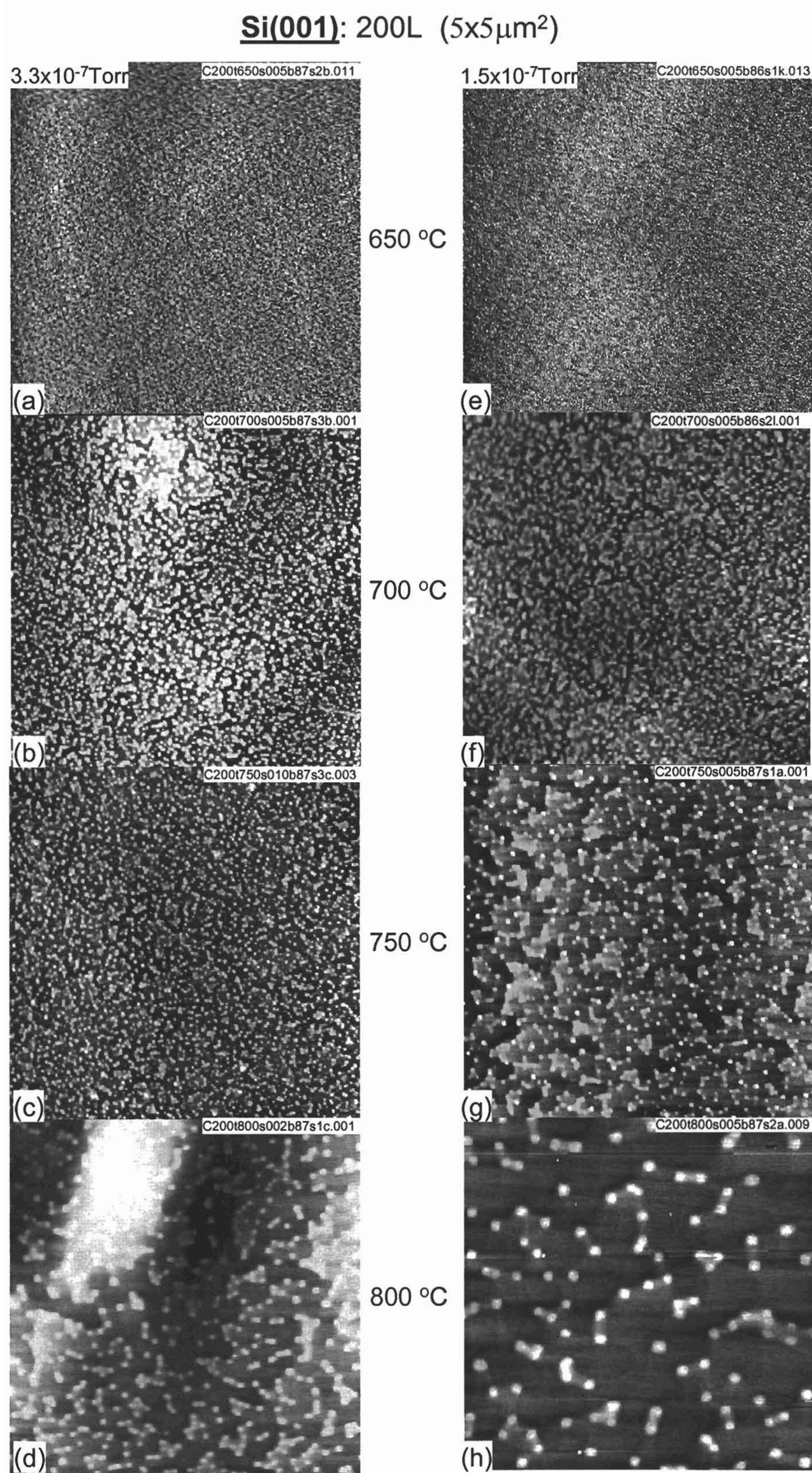

Fig. 2.3: AFM images (5×5 μm^2) of 200 L O_2/Si(001) as a function of temperature at (a–d) 3.3×10^{-7} Torr and (e–h) 1.5×10^{-7} Torr.

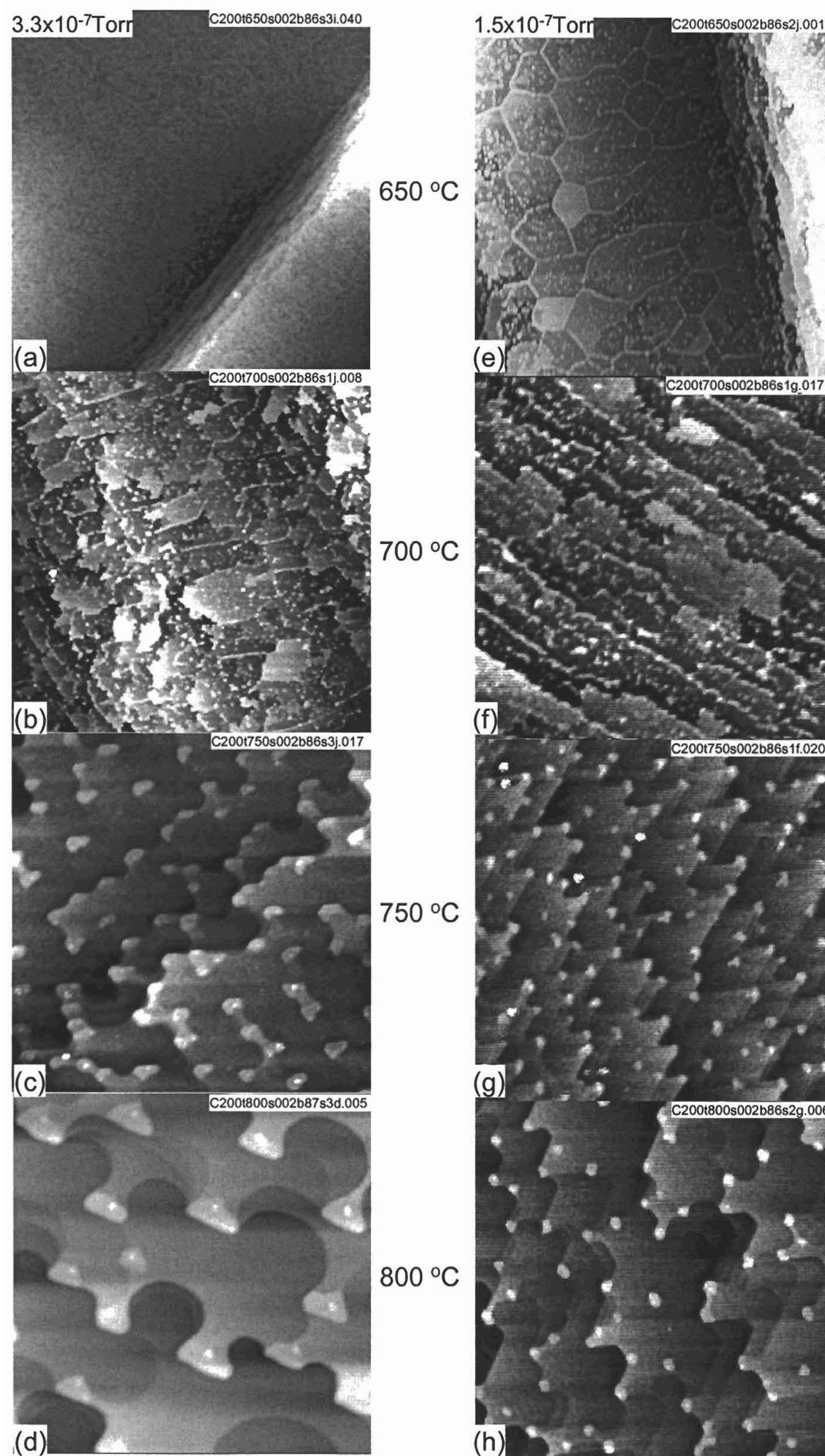

Fig. 2.4: AFM images (2×2 μm^2) of 200 L O_2/Si(111) as a function of temperature at (a–d) 3.3×10^{-7} Torr and (e–h) 1.5×10^{-7} Torr.

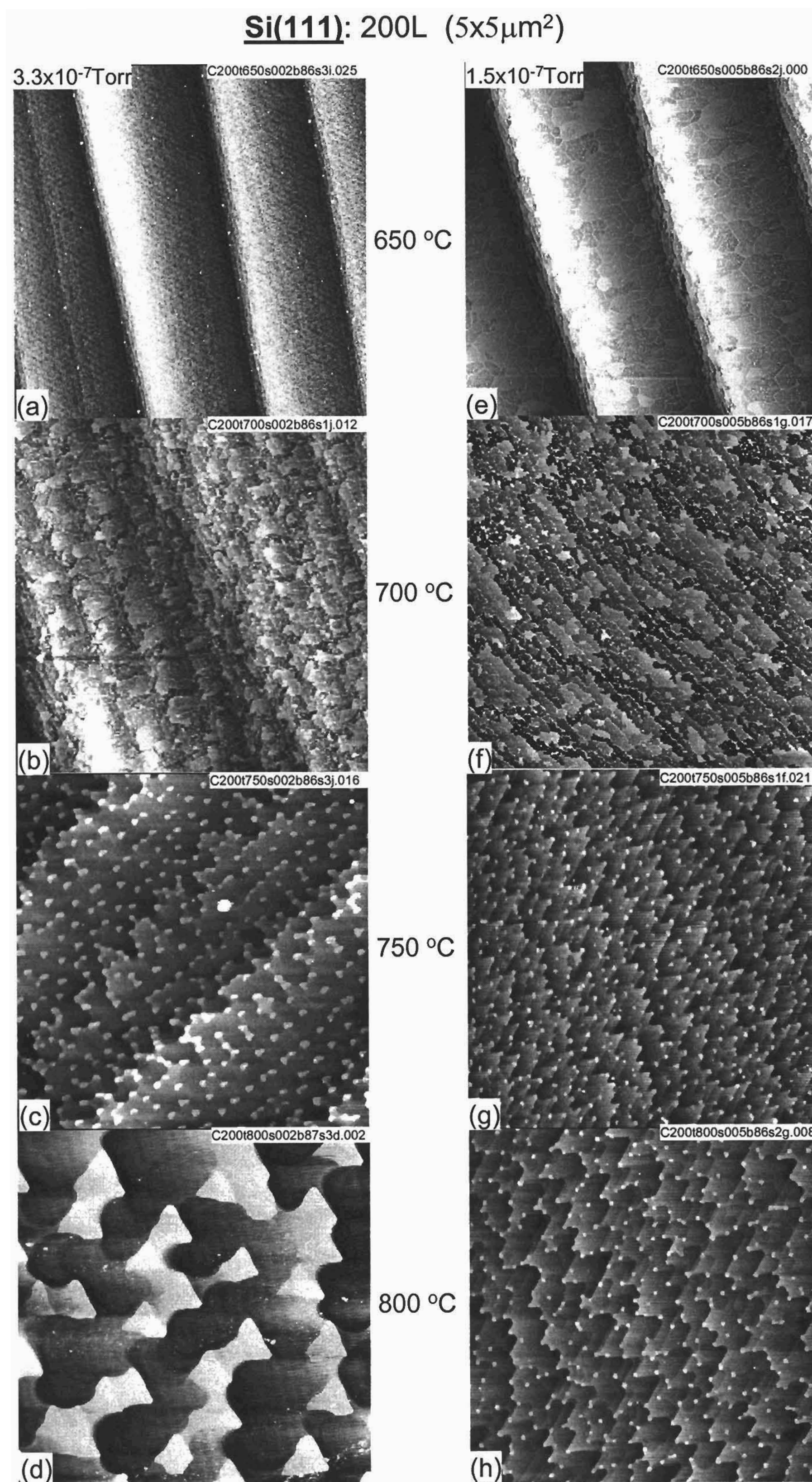

Fig. 2.5: AFM images (5×5 μm^2) of 200 L O_2/Si(111) as a function of temperature at (a–d) 3.3×10^{-7} Torr and (e–h) 1.5×10^{-7} Torr.

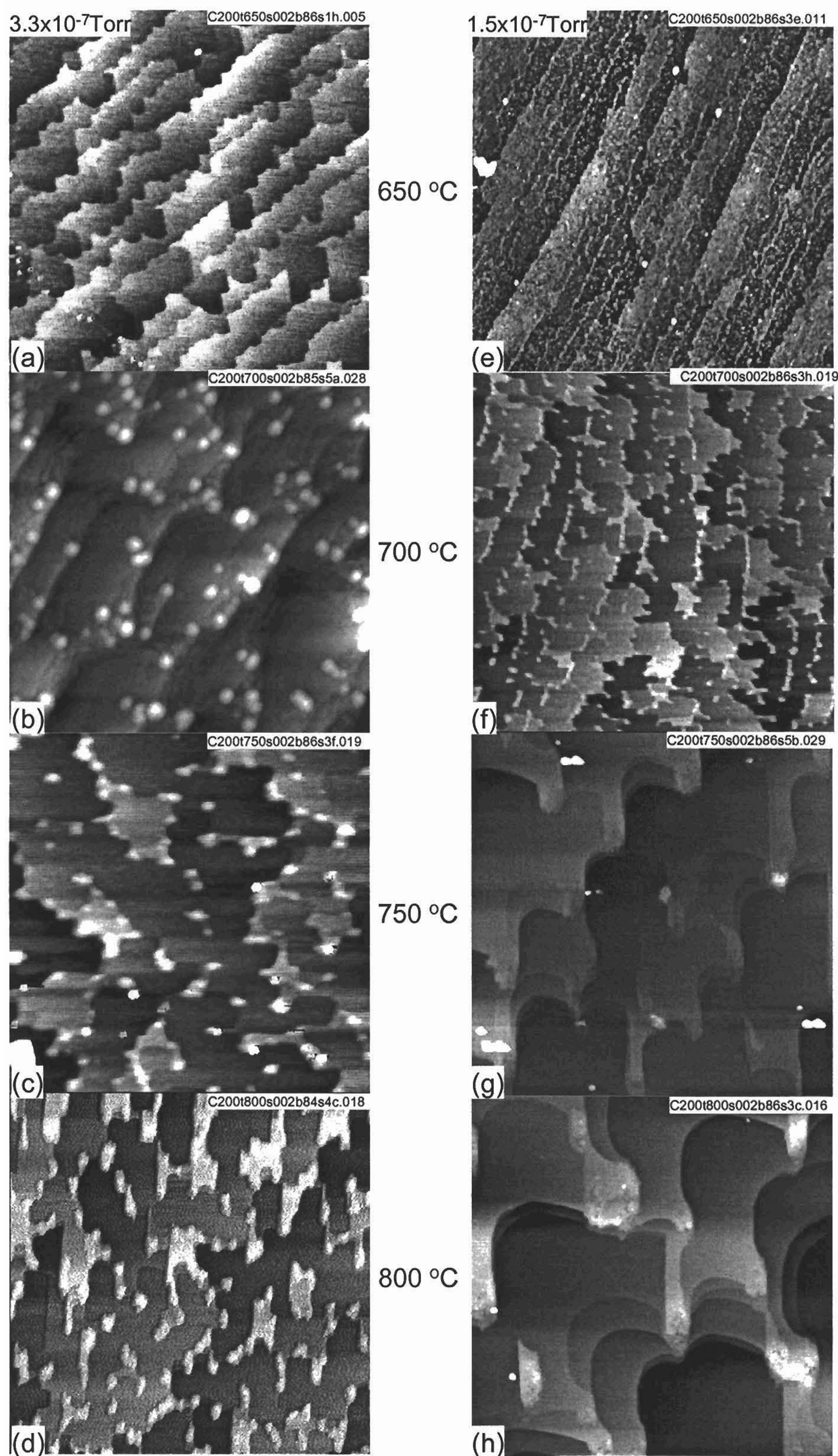

Fig. 2.6: AFM images ($2\times2\ \mu m^2$) of 200 L O_2/Si(113) as a function of temperature at (a–d) 3.3×10^{-7} Torr and (e–h) 1.5×10^{-7} Torr.

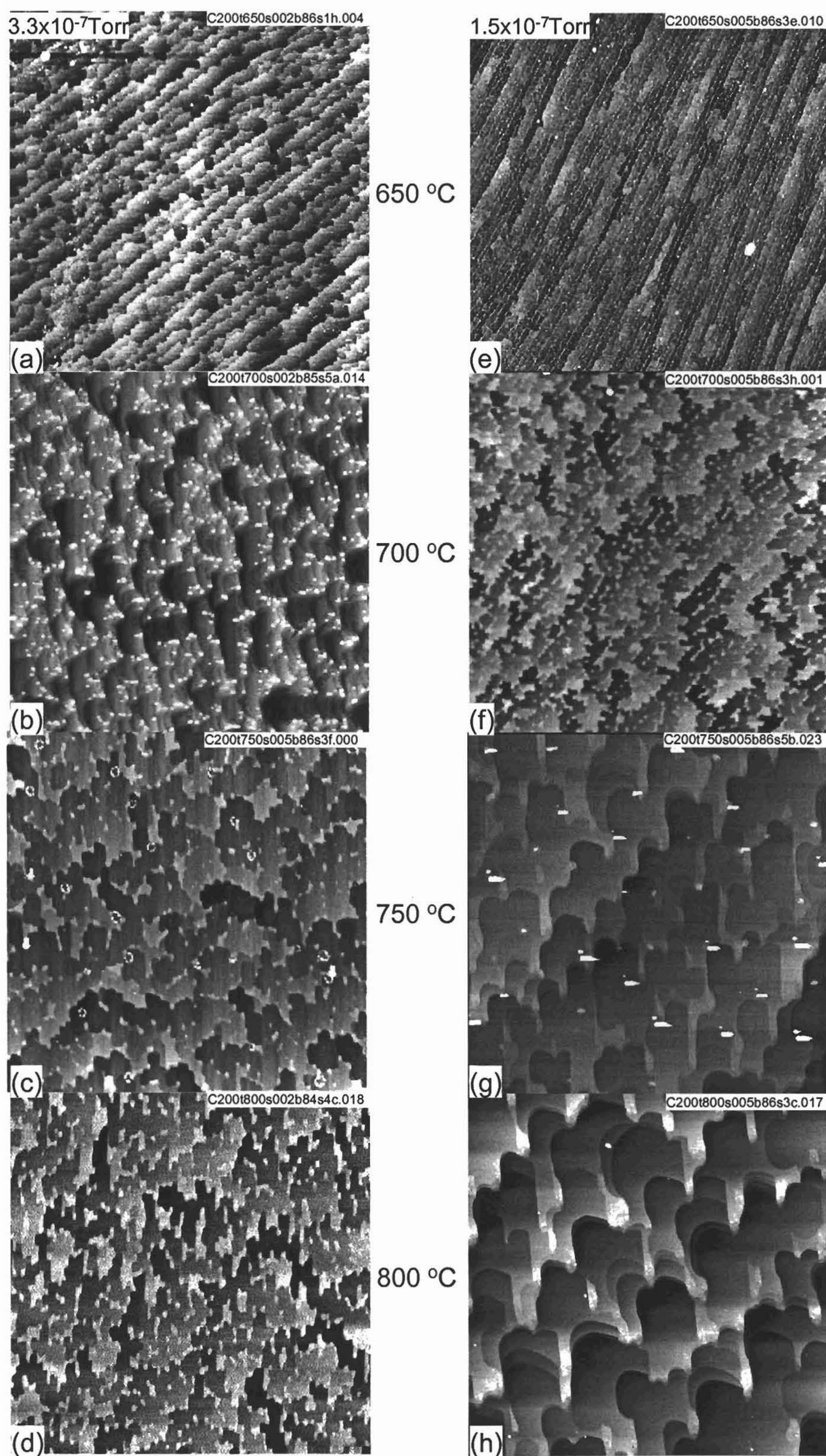

Fig. 2.7: AFM images (5×5 μm^2) of 200 L O_2/Si(113) as a function of temperature at (a–d) 3.3×10^{-7} Torr and (e–h) 1.5×10^{-7} Torr.

Chapter 3: Oxygen Etching of Unstable Si(5 5 12) and Si(112) Surfaces

In this chapter, we examine the two surface orientations that are not stable after extended oxygen etching: Si(5 5 12) and Si(112). This is not surprising since previous studies have shown that metal deposition causes faceting of Si(5 5 12) to more stable nearby orientations, and Si(112) does not form a stable, clean surface reconstruction. As will be shown, both Si(5 5 12) and Si(112) form row-like, sawtooth structures after etching that are primarily composed of more stable (111) and (113) planes (see Fig. 3.1). Again, temperature and pressure influence the resulting surface morphology, with feature sizes increasing in size at higher temperatures.

3.1 O_2 Etching of Si(5 5 12)

Unlike for the stable Si surfaces examined in Chapter 2, the Si(5 5 12) surface morphology changes quite dramatically during etching as a function of temperature. The initial clean Si(5 5 12) surface forms a stable reconstruction composed of row-like Si features. As shown in Fig. 3.2, the etched surface forms islands at lower temperatures with enhanced island nucleation at step edges (Fig. 3.2b,e). These step edge islands become elongated along the $[\bar{1}10]$ direction at temperatures above 700 °C, extending to form "fingers" oriented perpendicular to the steps (Fig. 3.2c,f). At higher temperatures, these fingers increase in length and height and lead to the formation of "sawtooth" facets that can be microns long (Fig. 3.2d,g,h). As expected, the size of the sawtooth facets increases and their density decreases at higher temperatures (compare Fig. 3.2g and 3.2h). At 750 °C (1.5×10^{-7} Torr), the sawtooths have an average width of 30 nm and length of 600 to 900 nm, and grow in size to ~90 nm wide and ~1600 nm long at 800 °C. Cross sections of the sawtooths formed at 800 °C are shown in Figs. 3.4 and 3.5 at intermediate (200 L) and high (400 L) exposure. At 200 L, some areas with (5 5 12) orientation still remain in the areas between sawtooths, which are composed of opposing (111) and (113)

planes. At 400 L, however, only the more stable (111) and (113) planes exist, indicating that the (5 5 12) orientation is not stable against extended oxygen etching.

3.2 O_2 Etching of Si(112)

The data presented here for oxygen etching of Si(112) are the first results for this system. Consequently, a larger variety of exposure conditions were explored. We examined etching at 3.3×10^{-7} Torr for temperatures from 750 °C to 950 °C and select coverages from 100 L to 800 L. This study begins at higher temperatures (750 °C) because Si(112) is an *unstable* surface orientation that forms nanofacets of (111) and (5 5 12)-like planes. Consequently, data at 750 °C shows island nucleation on nanofacets that produces a disordered surface (Fig. 3.6a,f). At 800 °C, the initial nanofacet morphology of the clean Si(112) surface is removed and significantly larger sawtooth facets dominate the surface. As expected, the size of these sawtooth facets increases and their density decreases with increasing temperature (compare Fig. 3.6b,g to 3.6e,j).

Figures 3.7 and 3.8 show the evolution of surface morphology as a function of exposure at 800 °C and 850 °C. These data sequences resemble "movies" of the surface as a function of time, where higher exposures correspond to longer times. At 800 °C, nanofacets of the clean surface are still present at 100 L, with some isolated nucleation of larger sawtooth facets commencing. With higher exposures, these sawtooth facets grow in size and density until they dominate the surface at 600 L (Fig. 3.7 d,h). At the higher temperature of 850 °C, the surface morphology evolves in a similar manner. One distinction, however, is that the regions between sawtooth facets appear qualitatively different. Figures 3.9 and 3.10 show cross sections of sawtooth structures for these two temperature regimes. In both cases, the sawtooths appear to be composed of opposing (113) and (111) planes, similar to sawtooths formed during etching of Si(5 5 12). Interestingly, at 800 °C these sawtooths are frequently separated by (112)-oriented flat regions, whereas at 850 °C they are separated by (5 5 12)-like terraces. This result

indicates that the (112) surface can be stabilized by etching at 800 °C, but is not stable with respect to the nearby (5 5 12) surface at higher temperatures. This result is quite interesting because it is the first time a nominally "clean" (112) surface has been observed.

3.3 Chapter 3 Figures

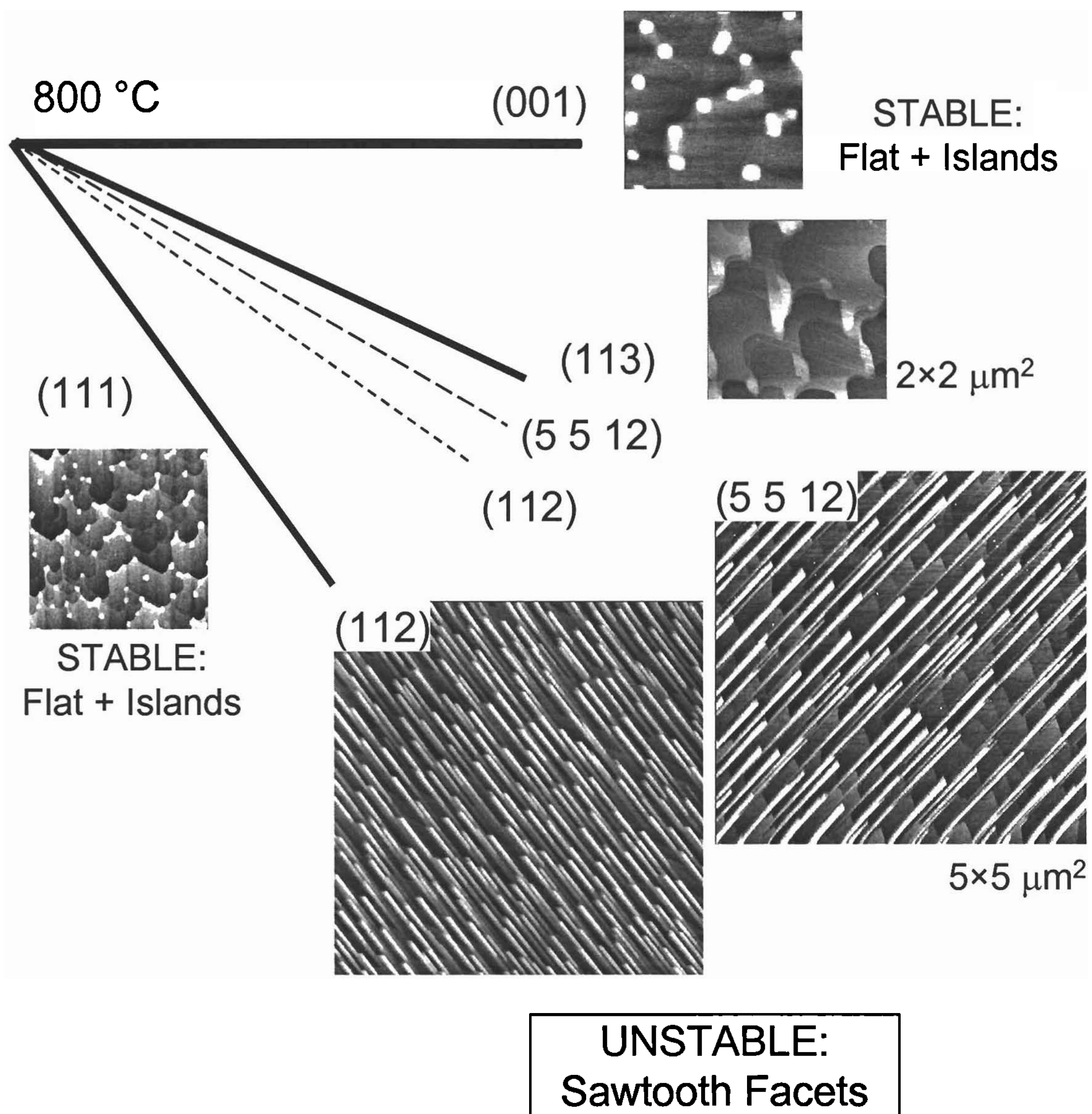

Fig. 3.1: Schematic of Si orientations with those surfaces unstable to oxygen etching highlighted: Si(112) and Si(5 5 12).

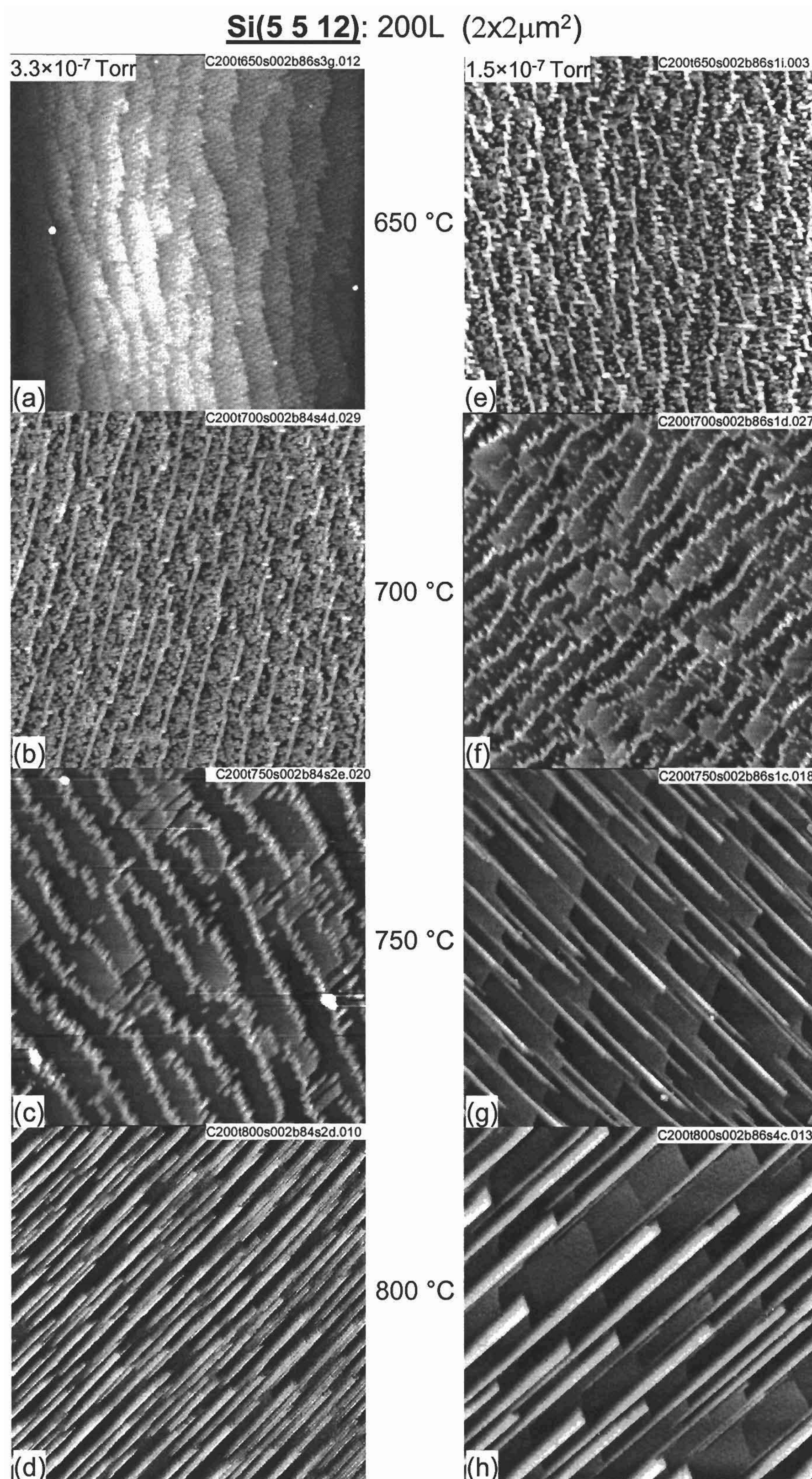

Fig. 3.2: AFM images (2×2 μm^2) of 200 L O_2/Si(5 5 12) as a function of temperature at (a-d) 3.3×10^{-7} Torr and (e-h) 1.5×10^{-7} Torr.

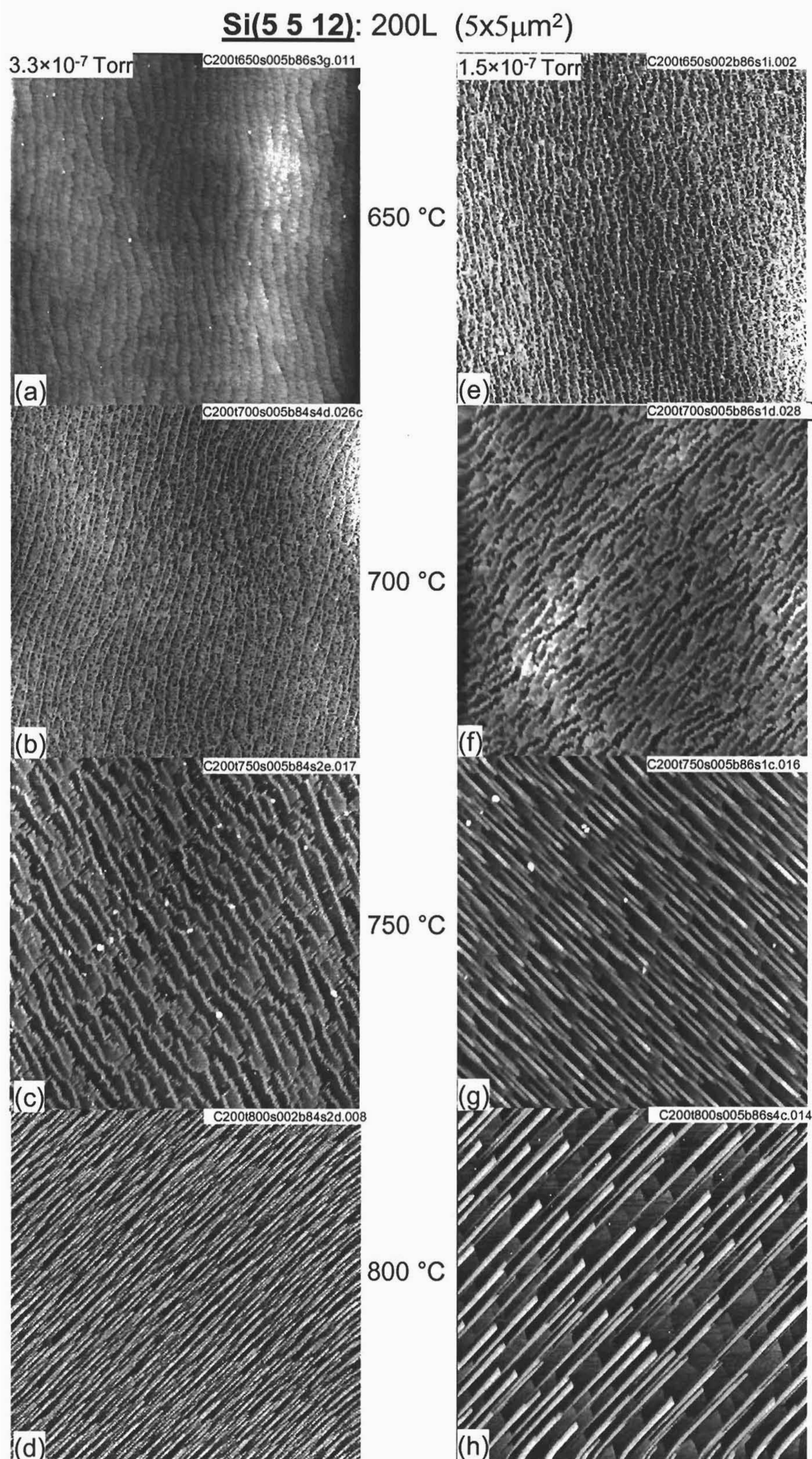

Fig. 3.3: AFM images (5×5 μm^2) of 200 L O_2/Si(5 5 12) as a function of temperature at (a-d) 3.3×10^{-7} Torr and (e-h) 1.5×10^{-7} Torr.

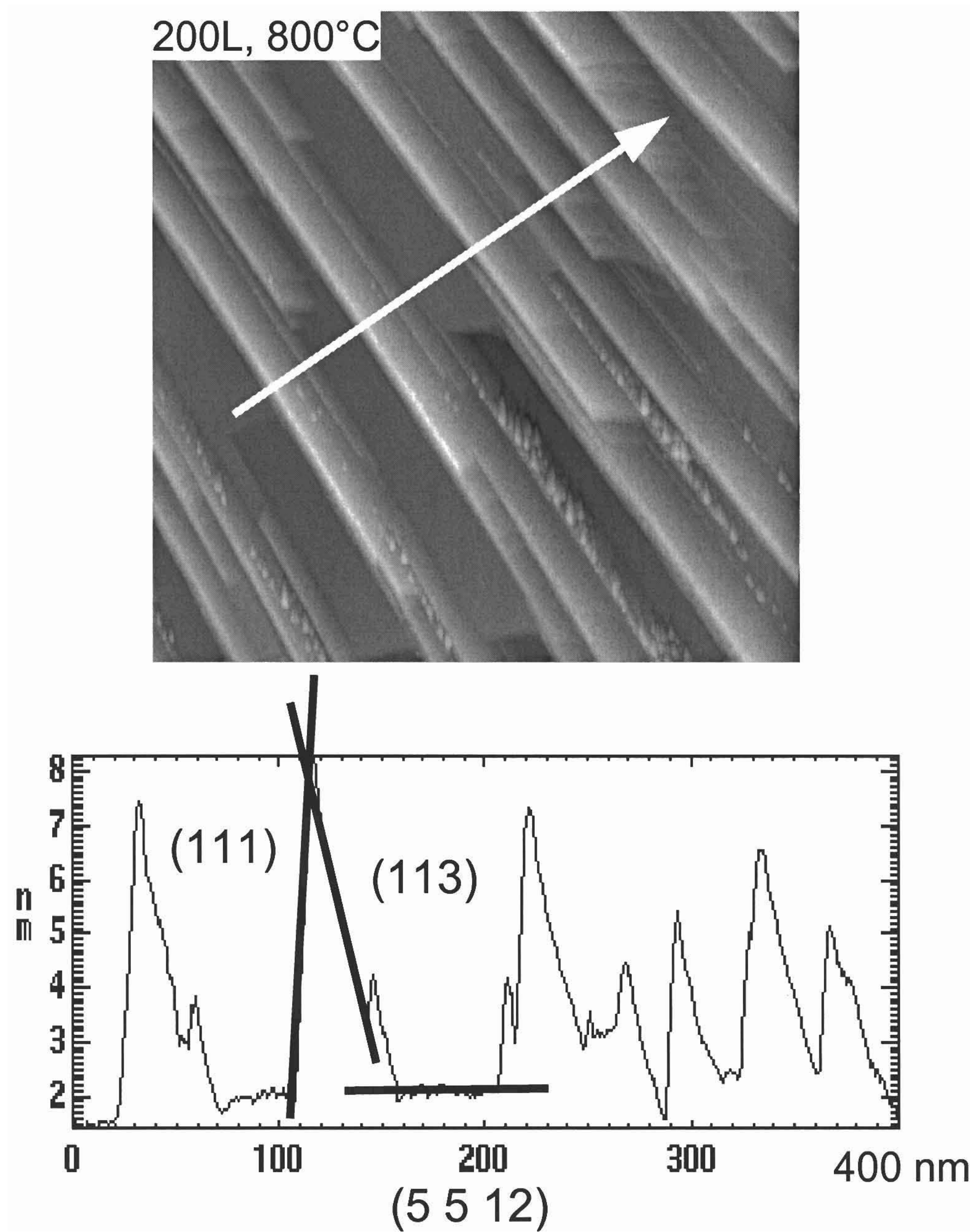

Fig. 3.4: Cross-section of "intermediate" sawtooth facets for O_2/Si(5 5 12) with 200 L at 800 °C.

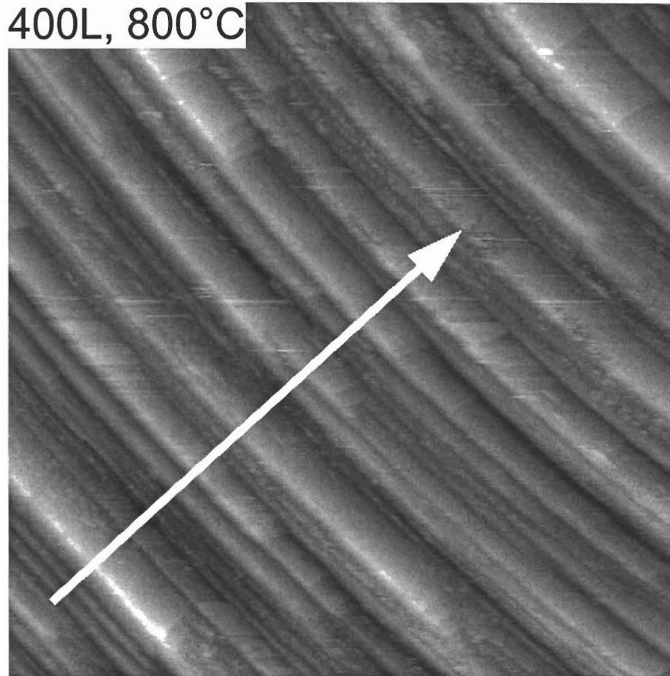

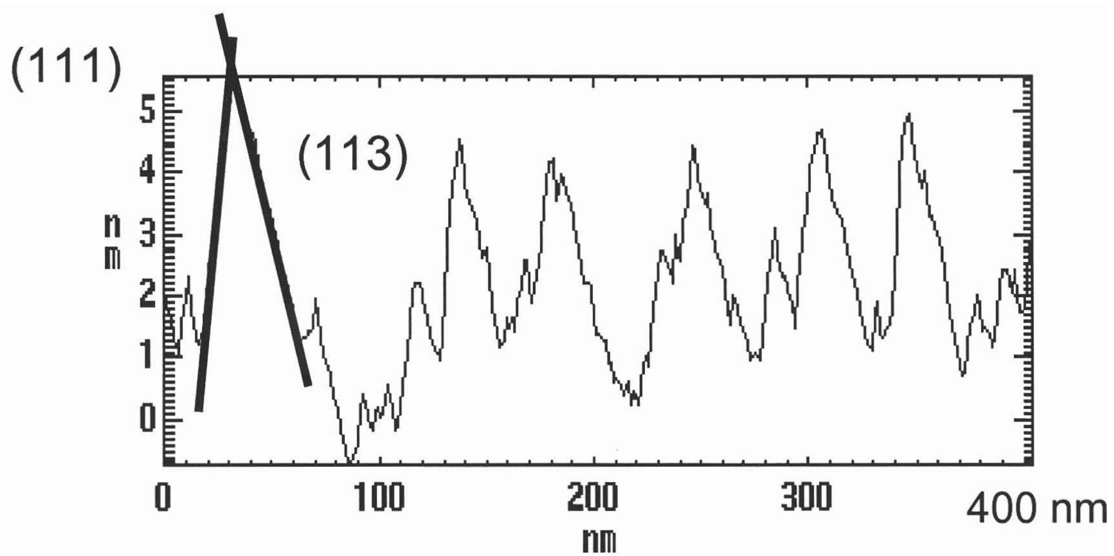

Fig. 3.5: Cross-section of "final" sawtooth facets for O_2/Si(5 5 12) with 400 L at 800 °C.

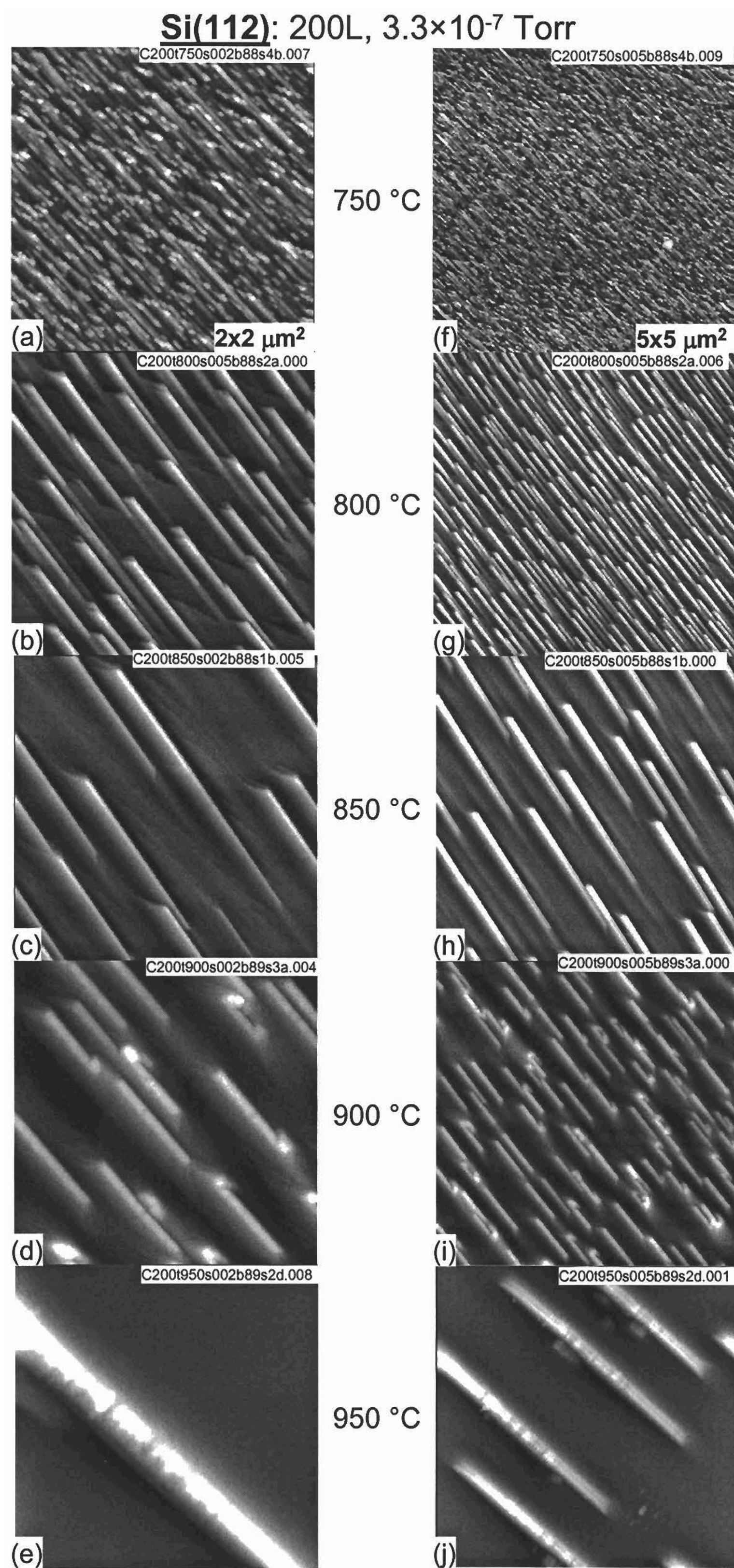

Fig. 3.6: (a-e) 2×2 μm^2 and (f-j) 5×5 μm^2 AFM images of 200 L O_2/Si(112) as a function of temperature at 3.3×10^{-7} Torr.

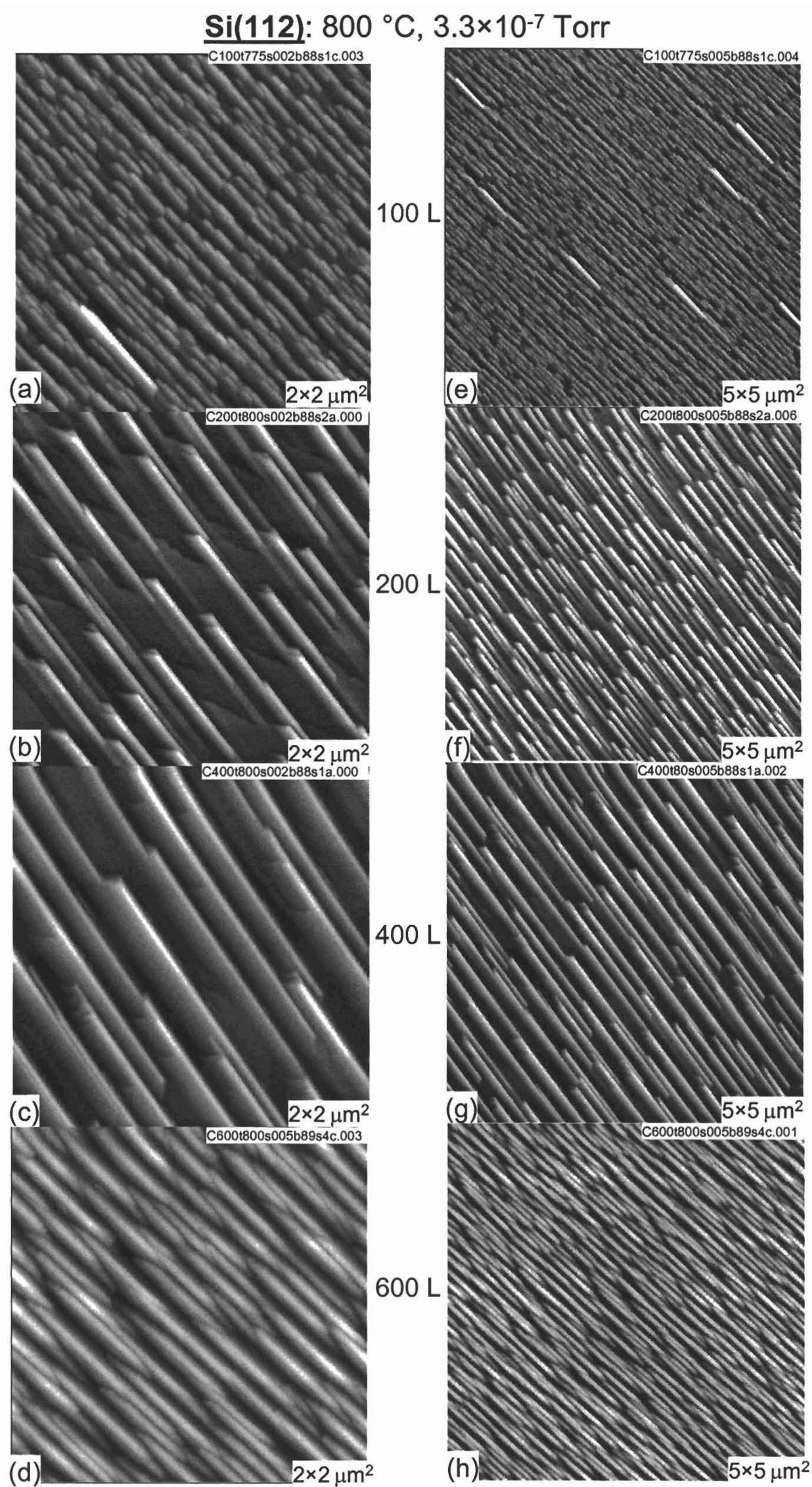

Fig. 3.7: (a-d) 2×2 μm^2 and (e-h) 5×5 μm^2 AFM images of O_2/Si(112) as a function of oxygen exposure at 3.3×10^{-7} Torr and 800 °C.

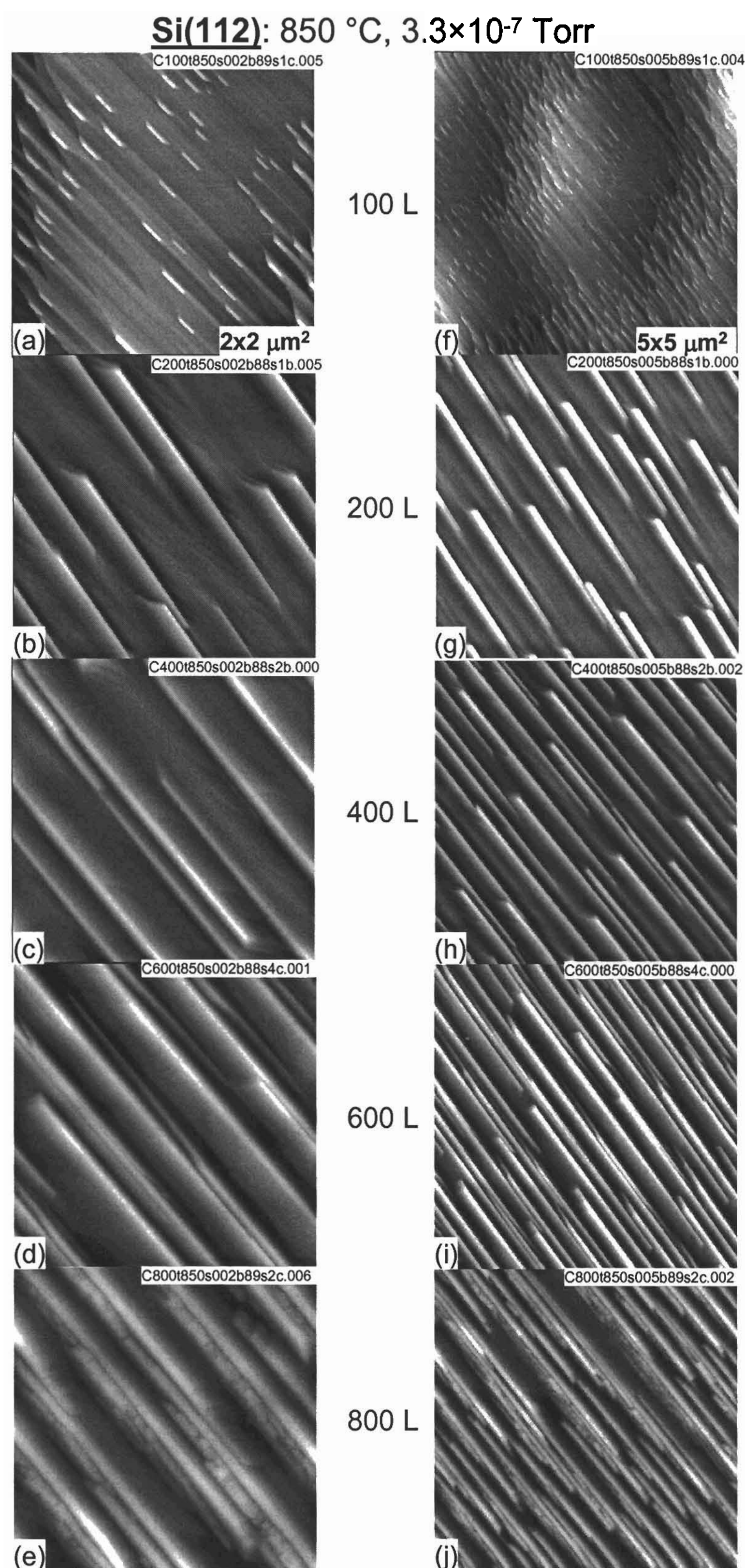

Fig. 3.8: (a-e) 2×2 μm^2 and (f-j) 5×5 μm^2 AFM images of O_2/Si(112) system as a function of exposure at 3.3×10^{-7} Torr and 850 °C.

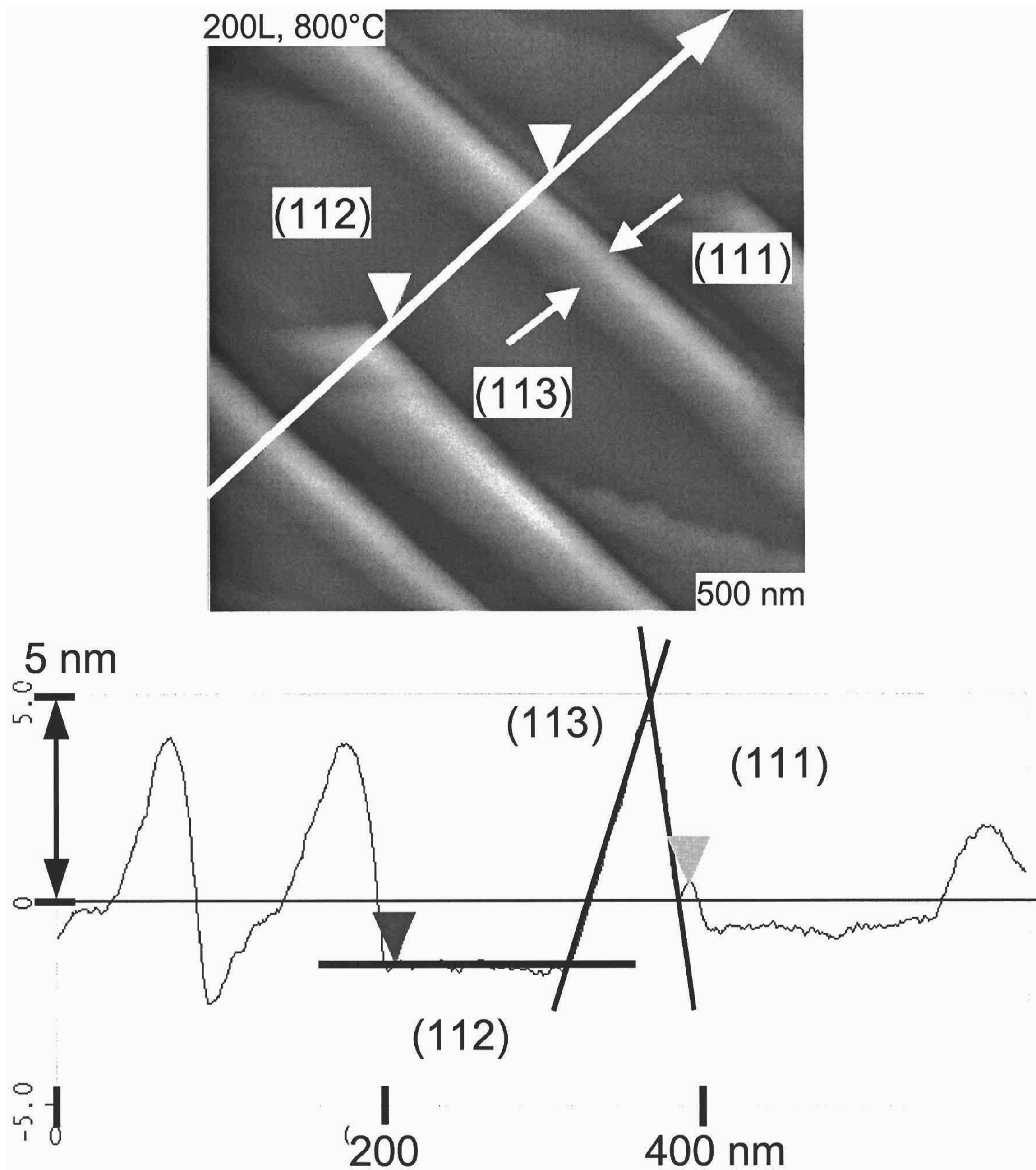

Fig. 3.9: Cross-section of "intermediate" sawtooth facets for O_2/Si(112) with 200 L at 800 °C.

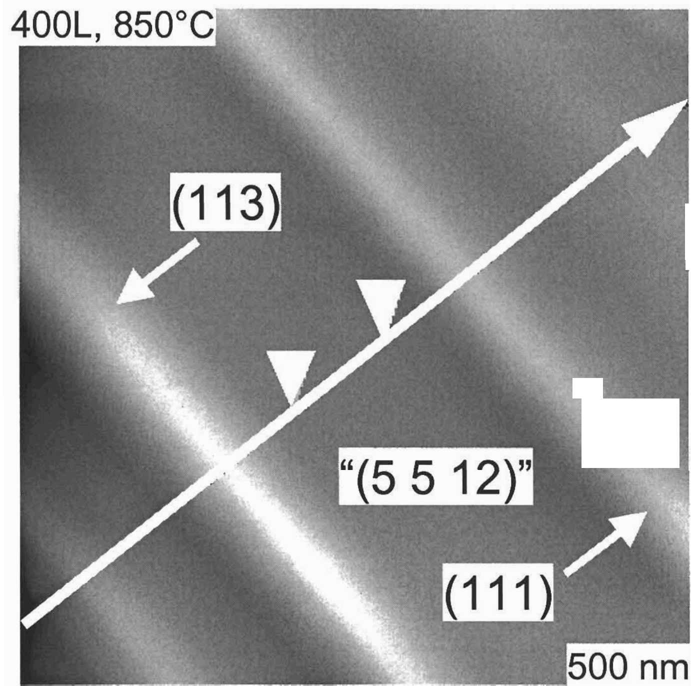

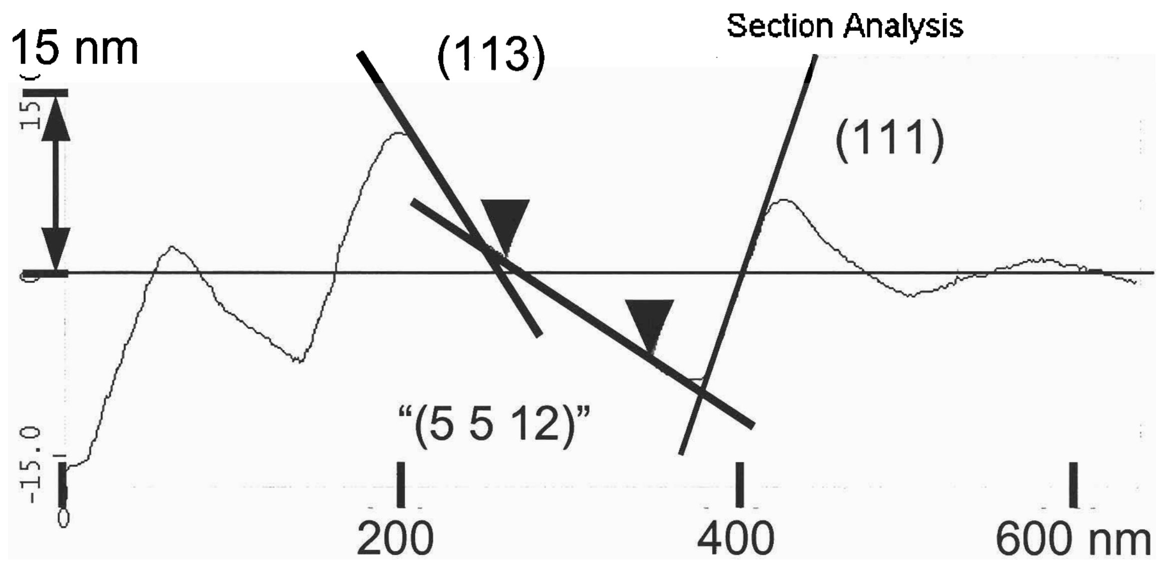

Fig. 3.10: Cross-section of "final" sawtooth facets for O_2/Si(112) with 400 L at 850 °C.

References

[1] G. Hollinger and F.J. Himpsel, Appl. Phys. Lett. **44**, 93 (1984).

[2] S. Hildebrandt, A. Kraus, R. Kulla, and H. Neddermeyer, Appl. Surf. Sci. **141**, 294 (1999).

[3] M Liehr, J.E. Lewis and G.W. Rubloff, J. Vac. Sci. Technol. A **5** 1559 (1987).

[4] G.W. Rubloff, J. Vac. Sci. Technol. A **8** 1857 (1990).

[5] T. Engel, Surf. Sci. Rep. **18**, 91 (1993).

[6] P. Morgen, U. Höfer, W. Wurth, and E. Umbach, Phys. Rev. B **39**, 3720 (1991).

[7] J.V. Seiple, C. Ebner, and J.P. Pelz, Phys. Rev. B **53**, 15432 (1996).

[8] J.V. Seiple and J.P. Pelz, Phys. Rev. Lett. **73**, 999 (1994).

[9] F.M. Leibsle, A. Samsavar, and T.-C. Chiang, Phys. Rev. B **38**, 5780 (1988).

[10] Y. Ono, M. Tabe, and H. Kageshima, Phys. Rev. B **48**, 14291 (1993).

[11] R. Tromp, G. W. Rubloff, P. Balk, and F.K. LeGoues, Phys. Rev. Lett. **55** 2332 (1985).

[12] M.A. Albao, D.-J. Liu, C.H. Choi, M.S. Gordon, and J.W. Evans, Surf. Sci. **555** 51 (2004).

[13] D.G. Cahill and Ph. Avouris, Appl. Phys. Lett. **60**, 326 (1992).

[14] Y.W. Mo, B.S. Swartzentruber, R. Karoitis, M.B. Webb, and M.C. Lagally, Phys. Rev. Lett. **63**, 2393 (1989).

[15] K.E. Johnson and T. Engel, Phys. Rev. Lett. **69**, 339 (1992).

[16] Ph. Avouris and D. Cahill, Ultramicroscopy **42-44**, 838 (1992).

[17] R. Kliese, B. Rottger, D. Bast, and H. Neddermeyer, Ultramicroscopy **42-44**, 824 (1992).

[18] K.E. Johnson, P.K. Wu, M. Sander, and T. Engel, Surf. Sci. **290**, 213 (1993).

[19] K. Wurm, R. Kliese, Y. Hong, B. Rottger, Y. Wei, H. Neddermeyer, and I.S.T. Tsong, Phys. Rev. B **50**, 1567 (1994).

[20] C. Ebner, J.V. Seiple, and J.P. Pelz, Phys. Rev. B **52**, 16651 (1995).

[21] J.V. Seiple and J.P. Pelz, J. Vac. Sci. Technol. A **13**, 772 (1995).

[22] V. Brichzin and J.P. Pelz, Phys. Rev. B **59**, 10138 (1999).

[23] Y. Chen, D.A.A. Ohlberg, G. Medeiros-Ribeiro, Y.A. Chang, and R.S. Williams, Appl. Phys. Lett. **76**, 4004 (2000).

[24] U. Köhler, J.E. Demuth, and R.J. Hamers, J. Vac. Sci. Technol. A **7**, 2860 (1989).

[25] H. Tokumoto, K. Miki, H. Murakami, H. Bando, M. Ono, and K. Kajimura, J. Vac. Sci. Technol. A **8**, 255 (1990).

[26] J.P. Pelz and R.H. Koch, Phys. Rev. B **42**, 3761 (1990).

[27] I.-W Lyo, Ph. Avouris, B Schubert and R. Hoffmann, J. Phys. Chem. **94**, 4400 (1990).

[28] J.P. Pelz and R.H. Koch, J. Vac. Sci. Technol. B **9**, 775 (1991).

[29] A. Feltz, U. Memmert, and R.J. Behm, Chem. Phys. Lett. **192**, 271 (1992).

[30] J. Seiple, J. Pecquet, Z. Meng, and J.P. Pelz, J. Vac. Sci. Technol. A **11**, 1649 (1993).

[31] A. Feltz, U. Memmert, and R.J. Behm, Surf. Sci. **314**, 34 (1994).

[32] T. Hasegawa, M. Kohno, S. Hosaka, and S. Hosoki, Surf. Sci. **312**, L753 (1994).

[33] R. Martel, Ph. Avouris, and I.-W. Lyo, Science, **272**, 385 (1996).

[34] G. Dujardin, A. Mayne, G. Comtet, L. Hellner, M. Jamet. E. Le Goff, and P. Millet, Phys. Rev. Lett. **76**, 3782 (1996).

[35] T. Engel, Surf. Sci. Rep. **18**, 91 (1993).

[36] H.H. Song, K.M. Jones, and A.A. Baski, J. Vac Sci. Technol. A **17**, 1696 (1999).

[37] A.A. Baski, K.M. Saoud, and K.M. Jones, Appl. Surf. Sci. **182**, 216 (2001).

[38] P.H. Woodworth, J.C. Moore, and A.A. Baski, J. Vac. Sci. Technol. A **21**, 1332 (2003).

[39] Jonathan Dickinson, Ph.D. Dissertation, Virginia Commonwealth University (2004).

APPENDIX A: AFM Images of Etched Si Surfaces (200 L)

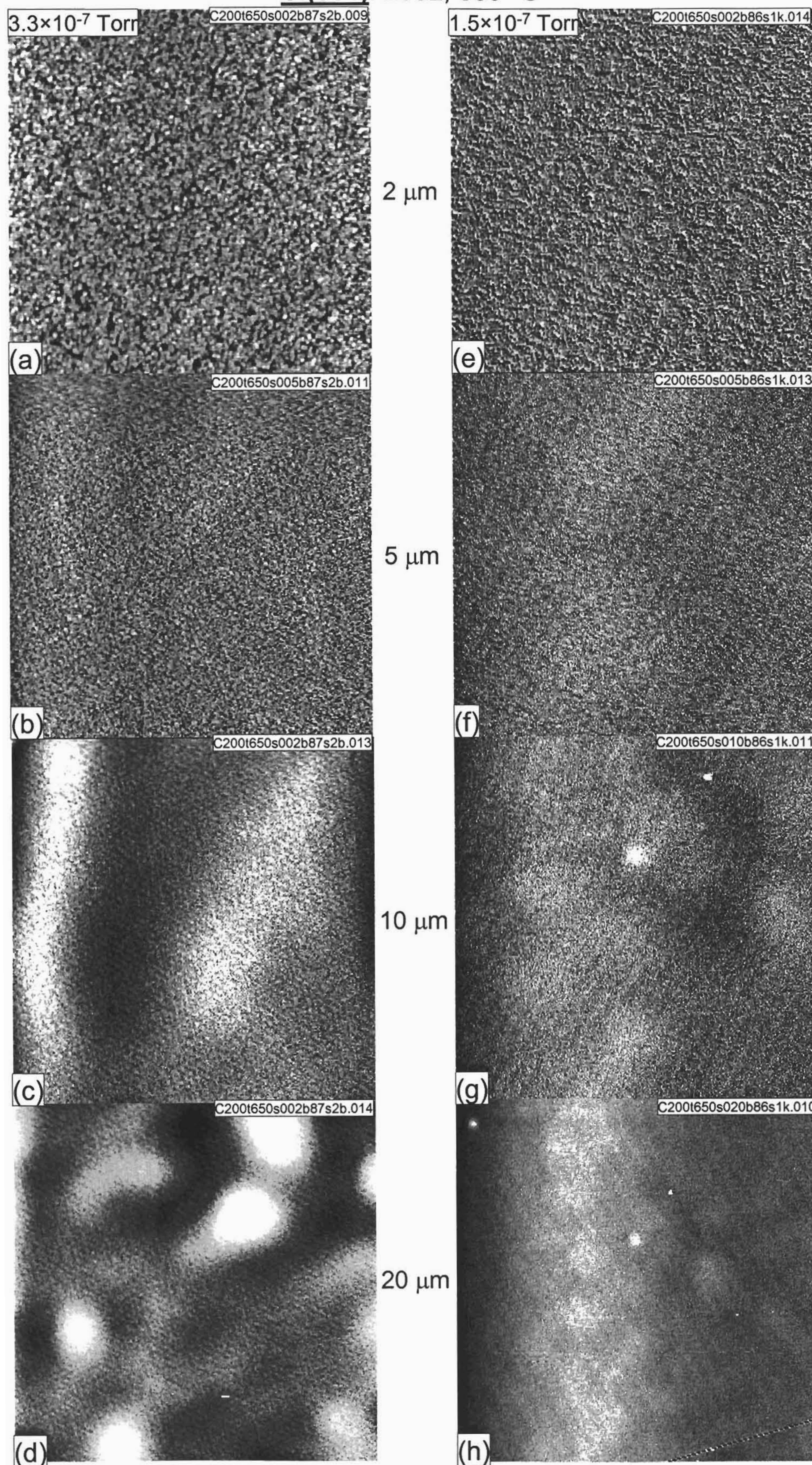

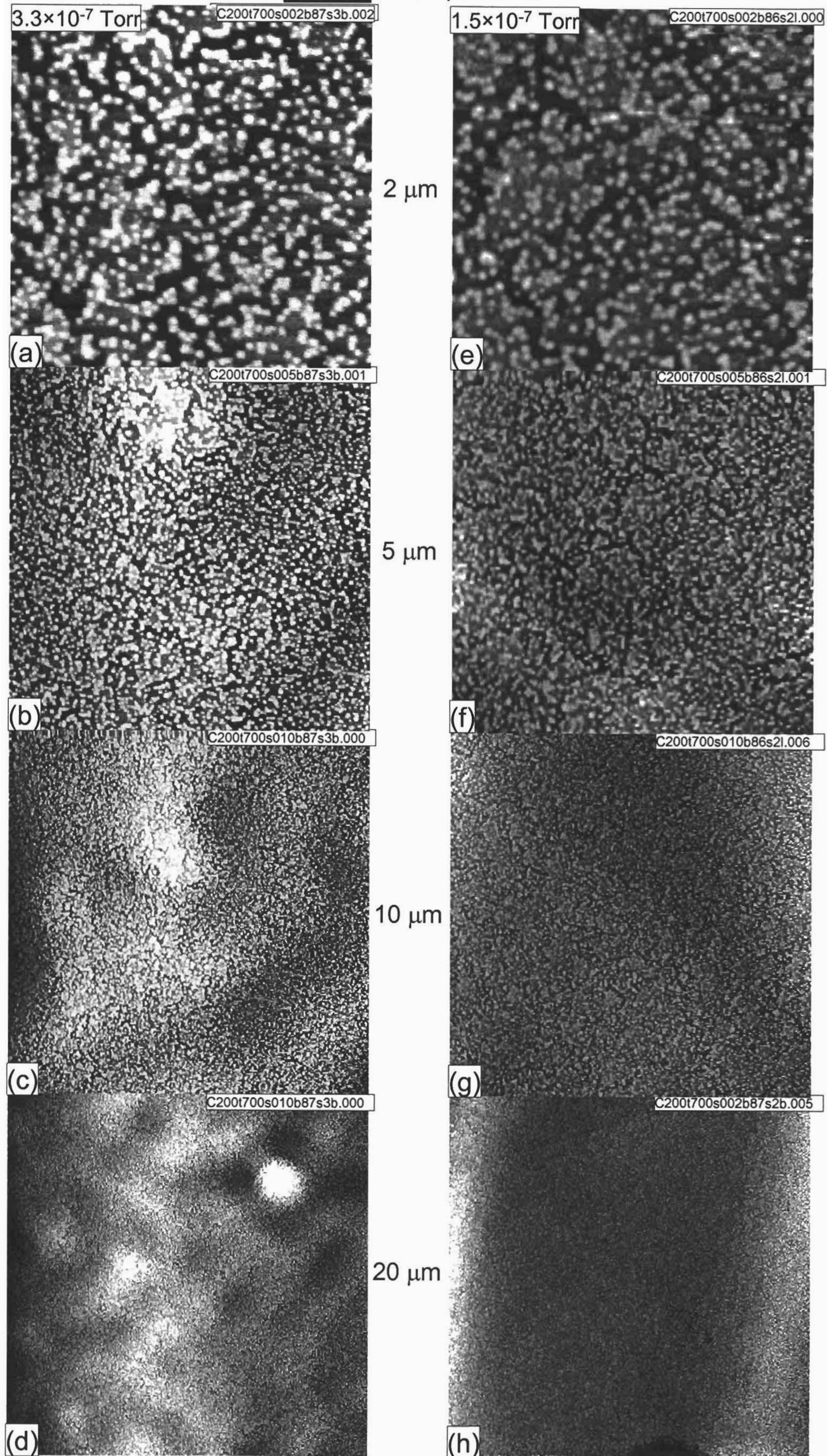

Appendix

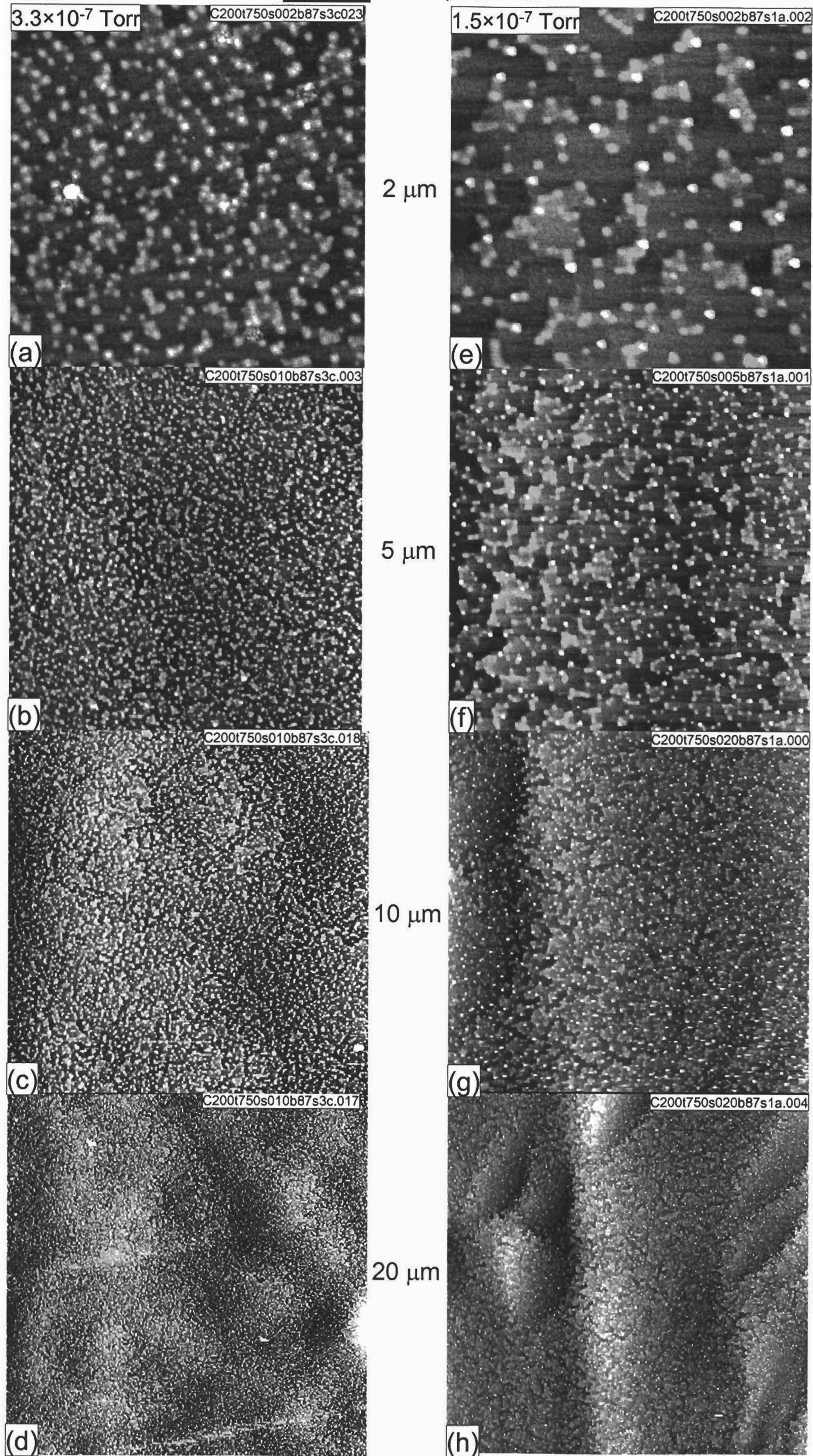
Si(001): 200L, 750 °C
3.3×10-7 Torr
C200t750s002b87s3c023
1.5×10-7 Torr
C200t750s002b87s1a.002
2 μm
(a)
(e)
C200t750s010b87s3c.003
C200t750s005b87s1a.001
5 μm
(b)
(f)
C200t750s010b87s3c.018
C200t750s020b87s1a.000
10 μm
(c)
(g)
C200t750s010b87s3c.017
C200t750s020b87s1a.004
20 μm
(d)
(h)

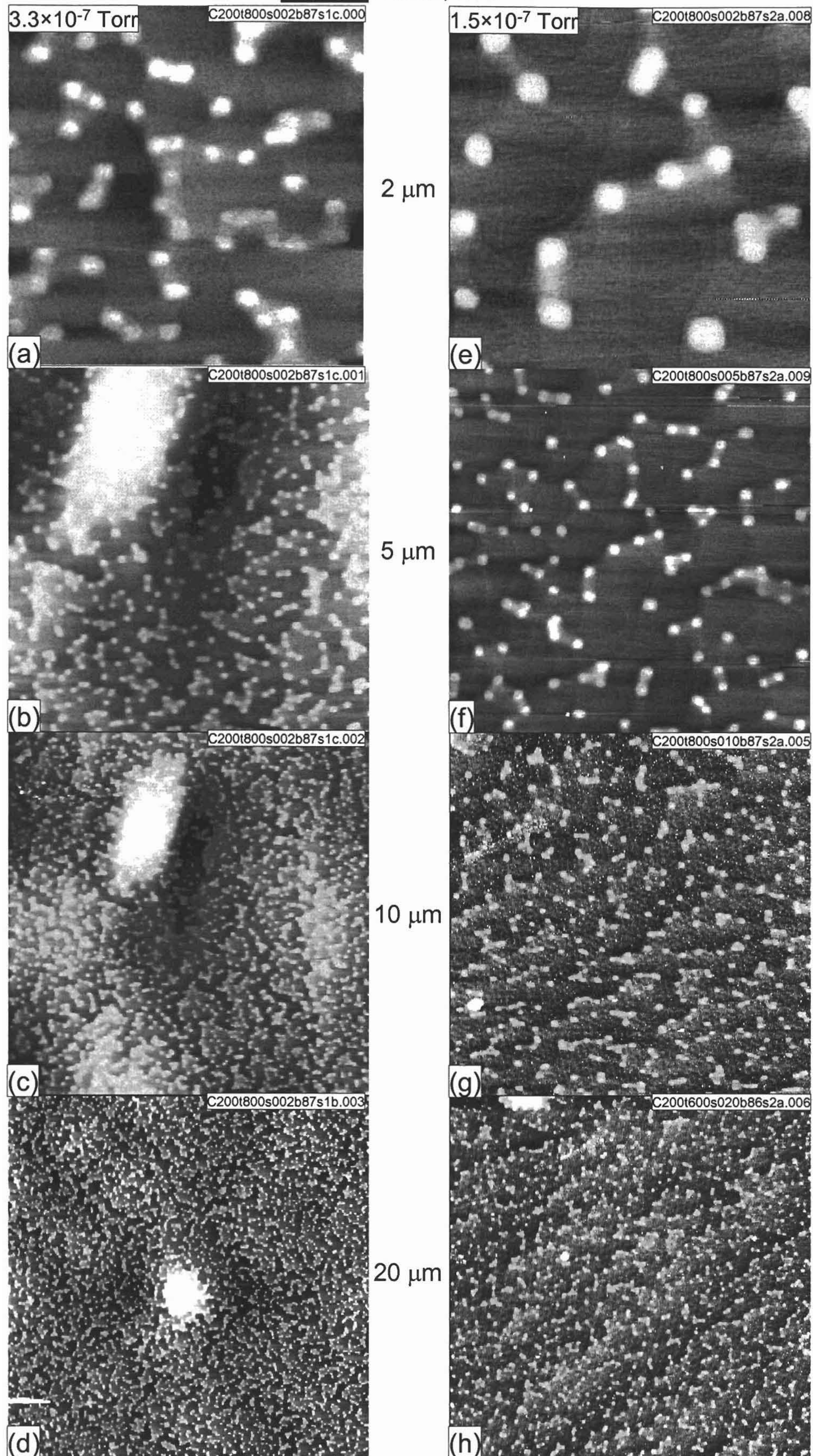
Si(001): 200L, 800 °C
3.3×10-7 Torr
C200t800s002b87s1c.000
1.5×10-7 Torr
C200t800s002b87s2a.008
2 μm
(a)
(e)
C200t800s002b87s1c.001
C200t800s005b87s2a.009
5 μm
(b)
(f)
C200t800s002b87s1c.002
C200t800s010b87s2a.005
10 μm
(c)
(g)
C200t800s002b87s1b.003
C200t600s020b86s2a.006
20 μm
(d)
(h)

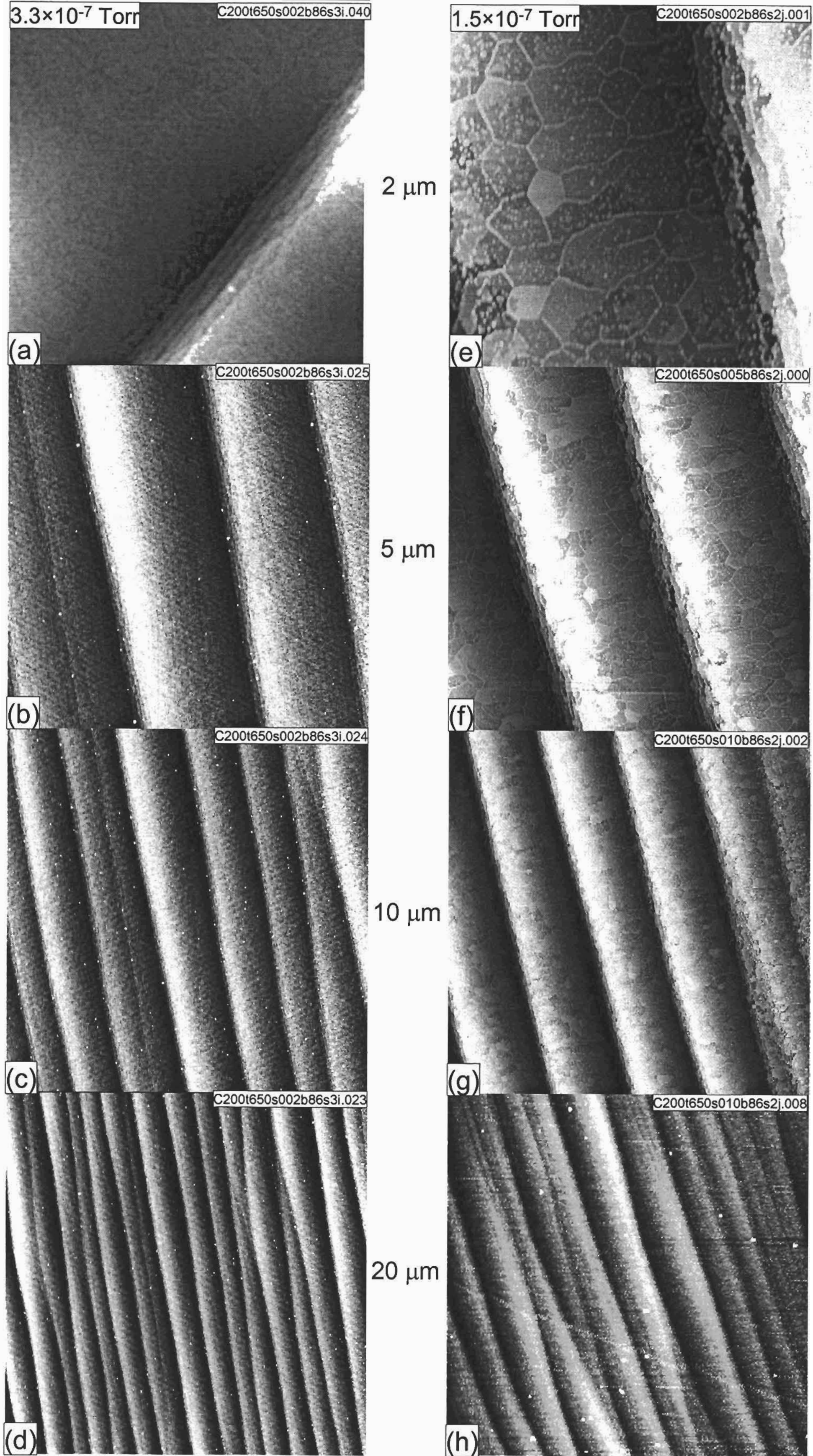
Si(111): 200L, 650 °C
3.3×10-7 Torr
C200t650s002b86s3i.040
1.5×10-7 Torr
C200t650s002b86s2j.001
2 μm
(a)
(e)
C200t650s002b86s3i.025
C200t650s005b86s2j.000
5 μm
(b)
(f)
C200t650s002b86s3i.024
C200t650s010b86s2j.002
10 μm
(c)
(g)
C200t650s002b86s3i.023
C200t650s010b86s2j.008
20 μm
(d)
(h)

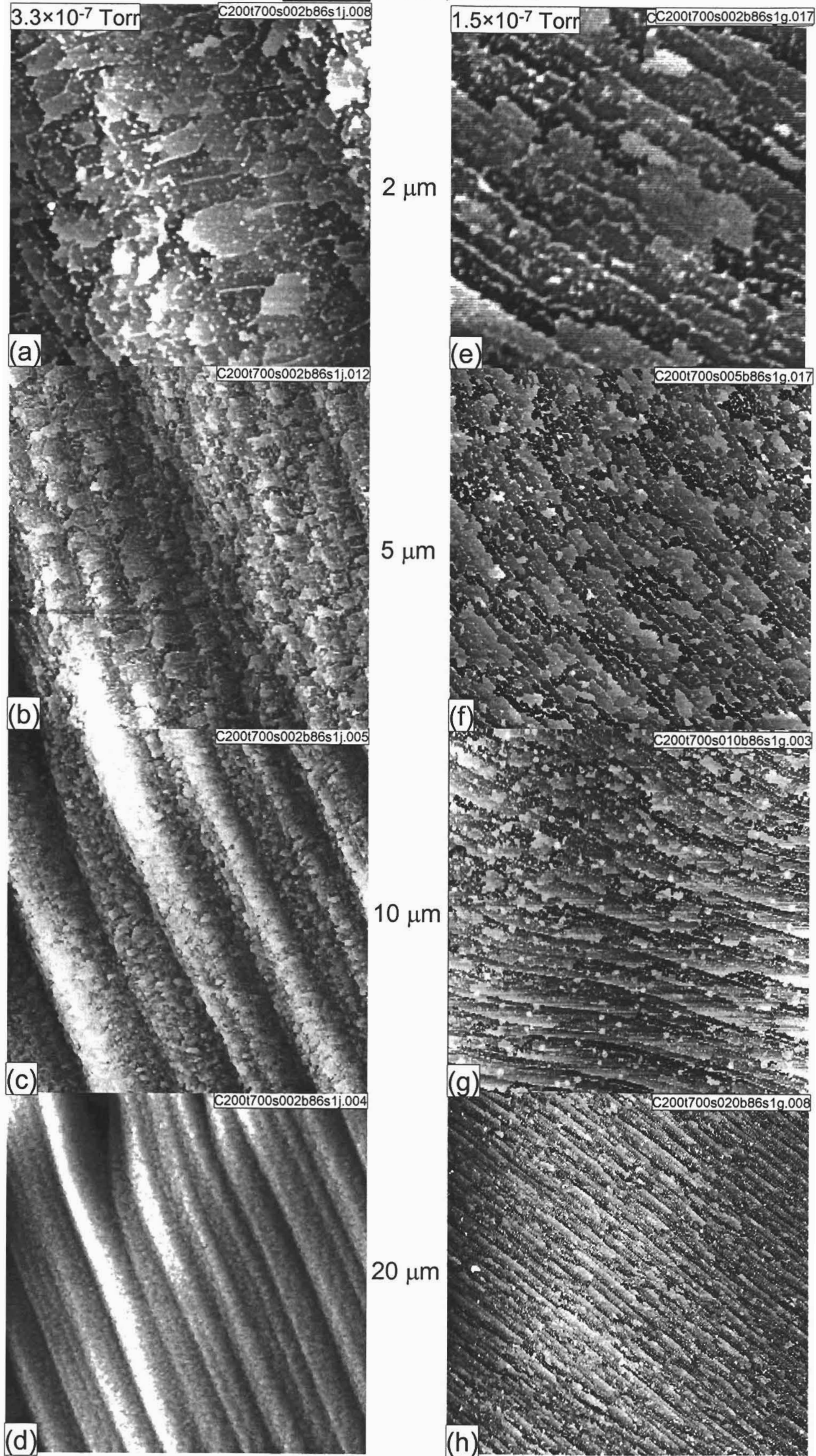
Si(111): 200L, 700 °C
3.3×10-7 Torr
1.5×10-7 Torr
C200t700s002b86s1j.008
C200t700s002b86s1g.017
2 μm
(a)
(e)
C200t700s002b86s1j.012
C200t700s005b86s1g.017
5 μm
(b)
(f)
C200t700s002b86s1j.005
C200t700s010b86s1g.003
10 μm
(c)
(g)
C200t700s002b86s1j.004
C200t700s020b86s1g.008
20 μm
(d)
(h)

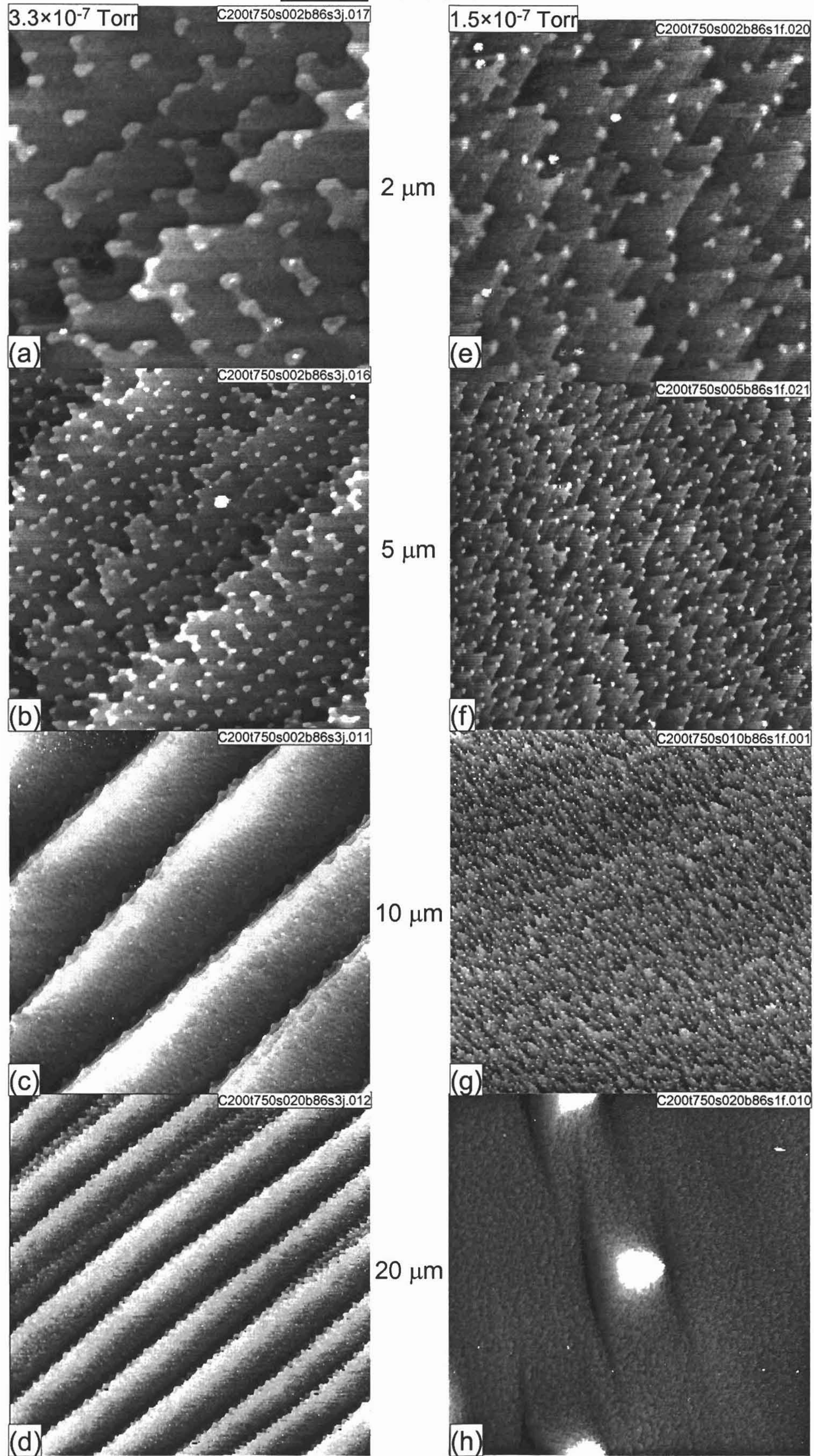

Appendix A.7

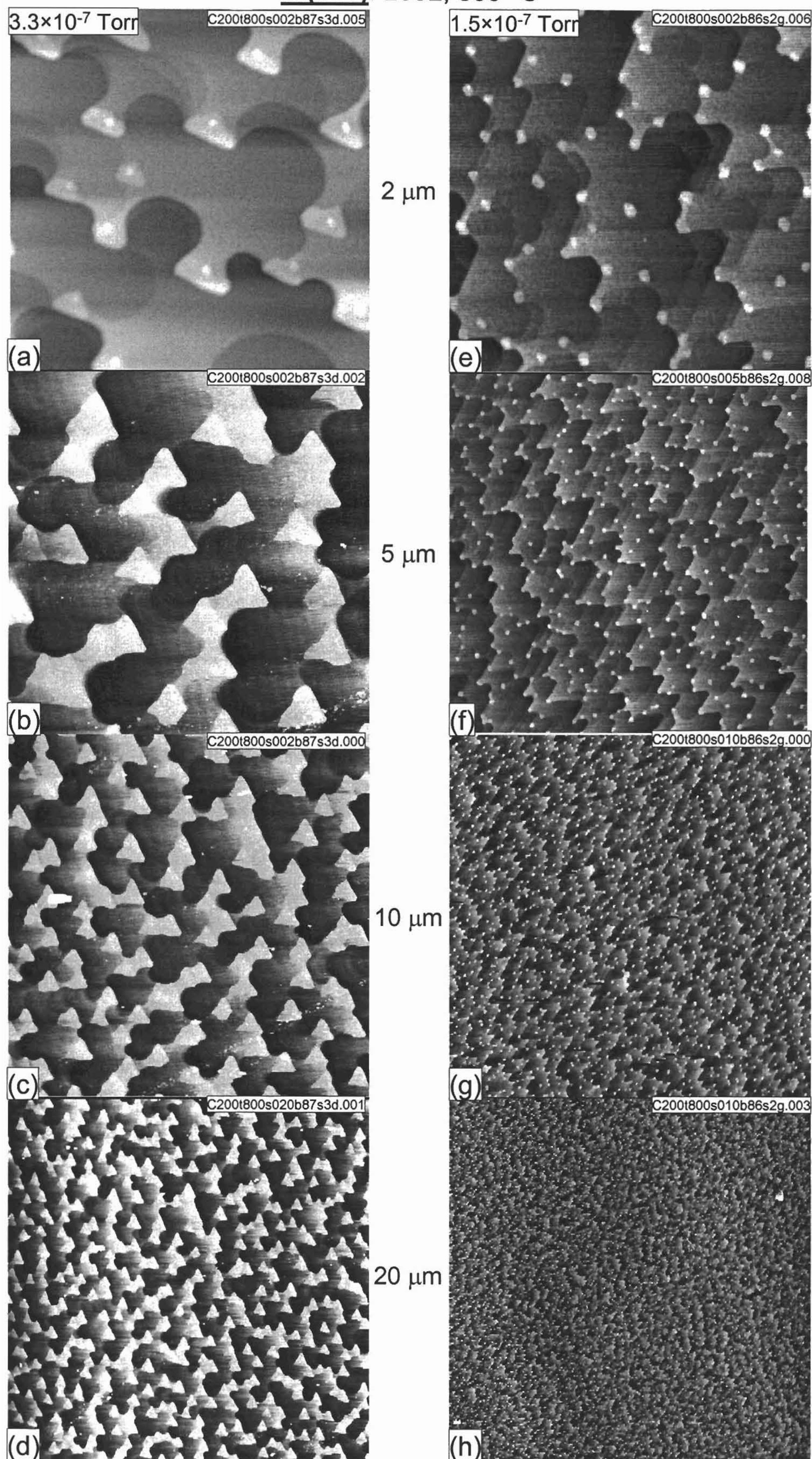

Appendix

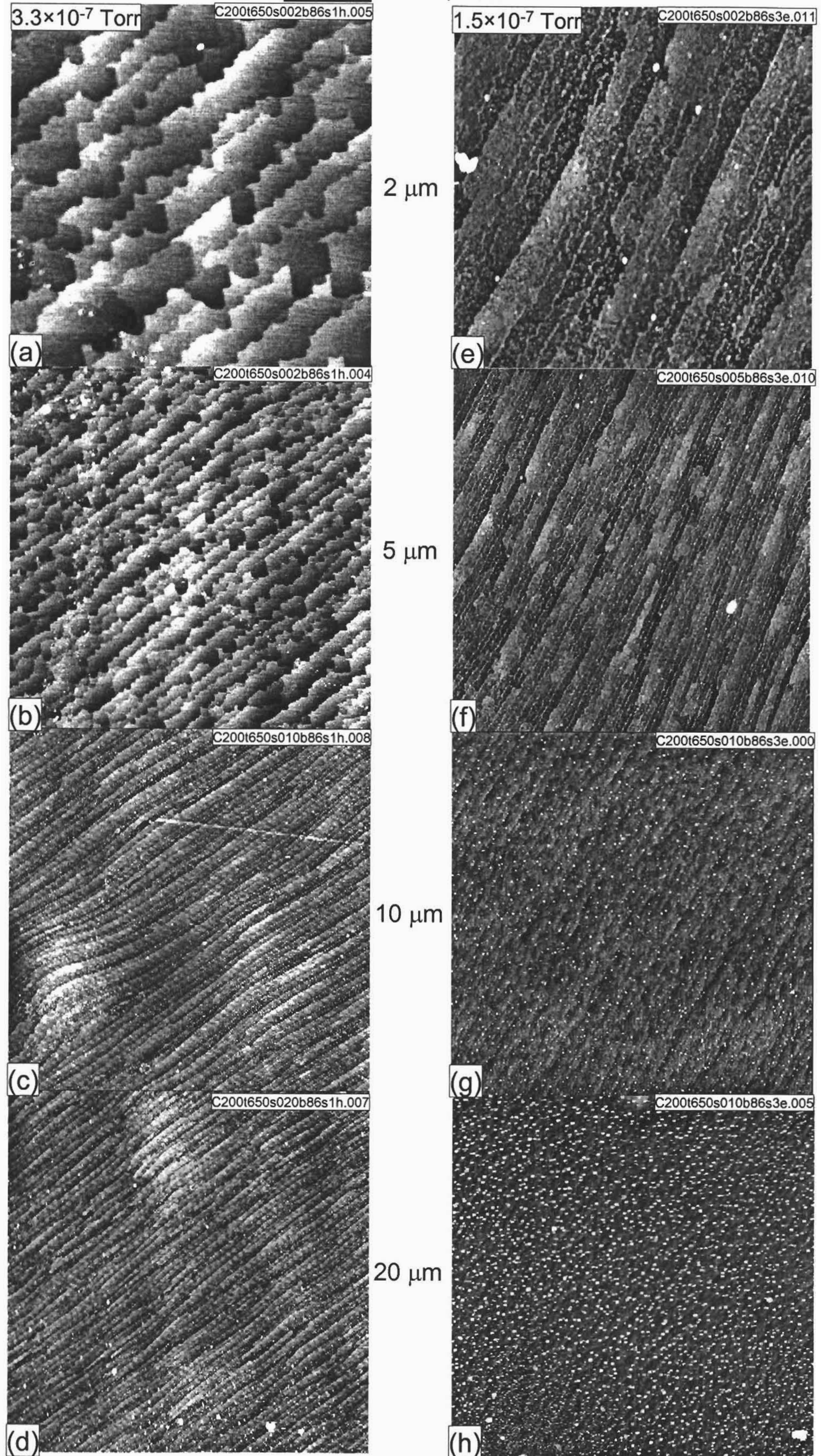

Appendix A.9

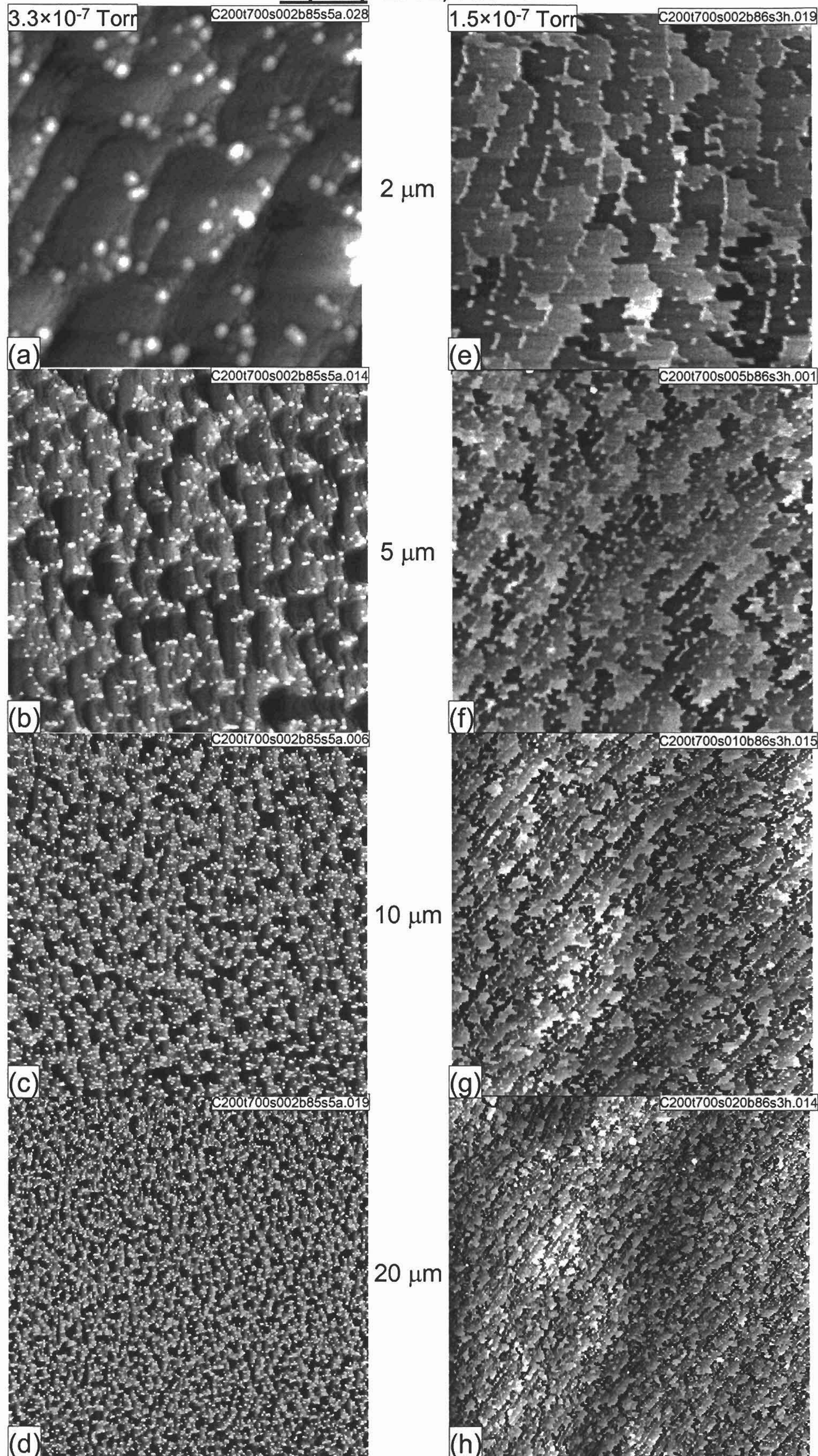

Si(113): 200L, 700 °C
3.3×10^-7 Torr
1.5×10^-7 Torr
C200t700s002b85s5a.028
C200t700s002b86s3h.019
2 μm
(a)
(e)
C200t700s002b85s5a.014
C200t700s005b86s3h.001
5 μm
(b)
(f)
C200t700s002b85s5a.006
C200t700s010b86s3h.015
10 μm
(c)
(g)
C200t700s002b85s5a.019
C200t700s020b86s3h.014
20 μm
(d)
(h)

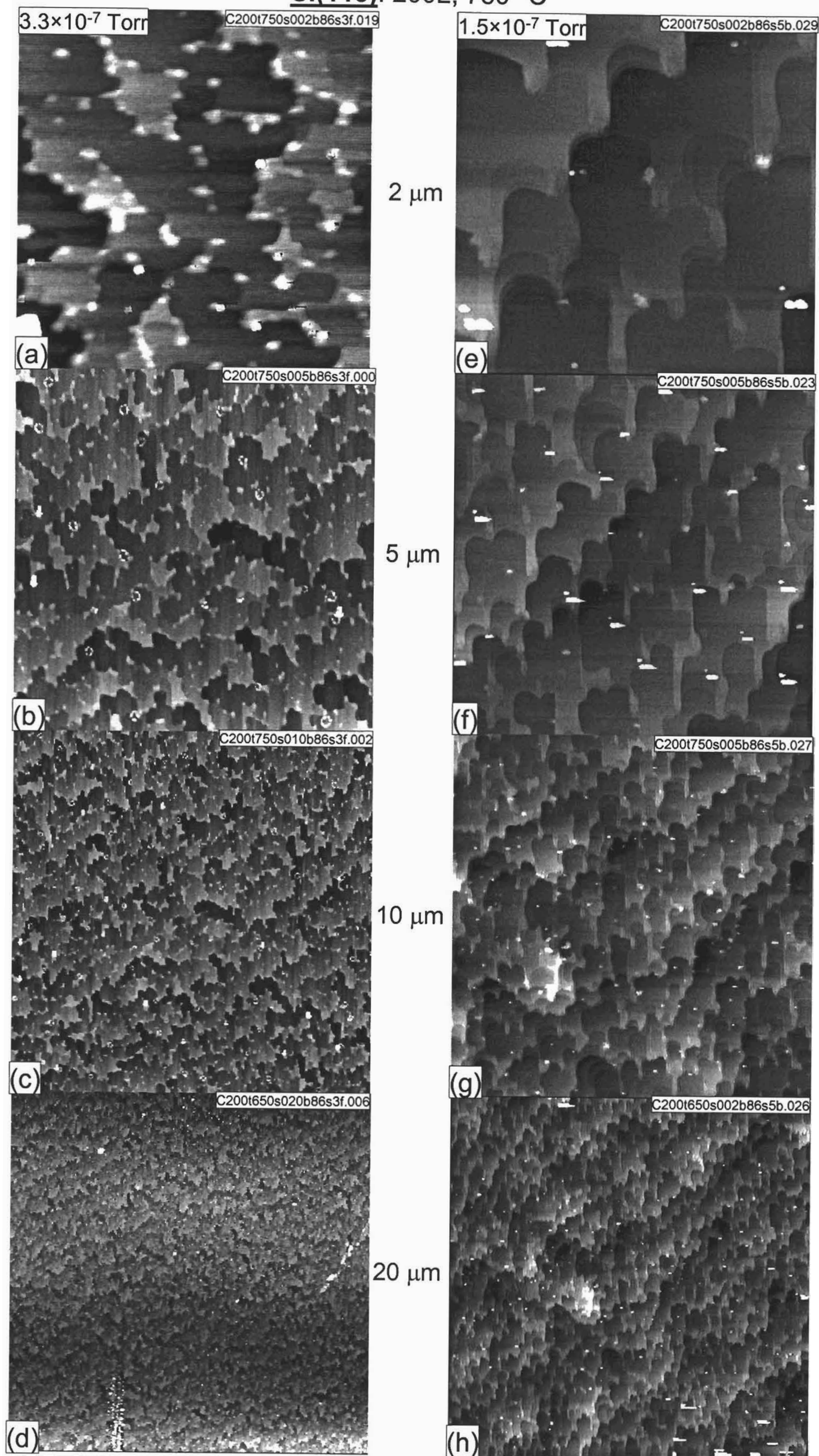
Si(113): 200L, 750 °C
3.3×10-7 Torr
C200t750s002b86s3f.019
1.5×10-7 Torr
C200t750s002b86s5b.029
2 μm
(a)
(e)
C200t750s005b86s3f.000
C200t750s005b86s5b.023
5 μm
(b)
(f)
C200t750s010b86s3f.002
C200t750s005b86s5b.027
10 μm
(c)
(g)
C200t650s020b86s3f.006
C200t650s002b86s5b.026
20 μm
(d)
(h)

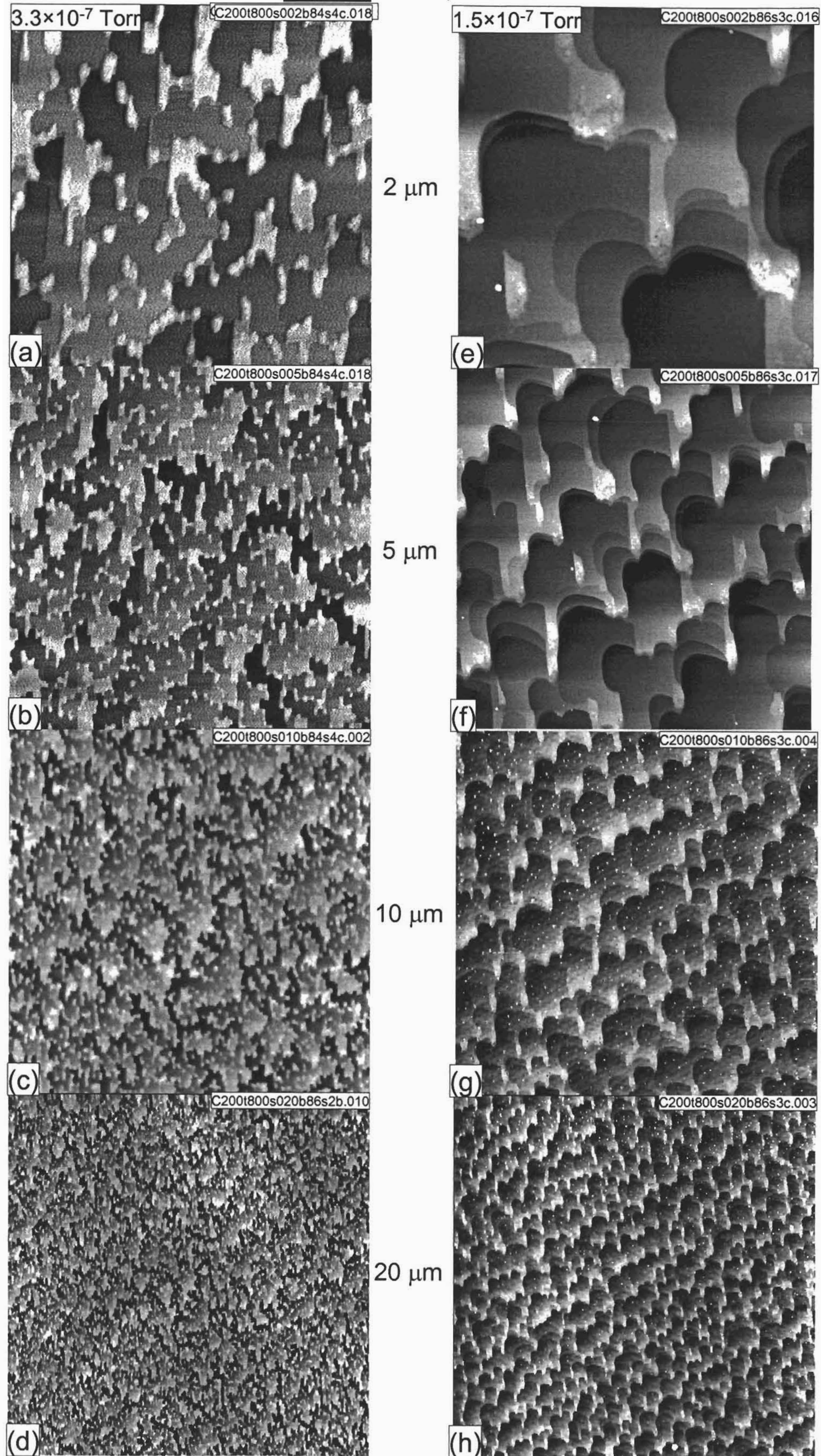

Appendix A.12

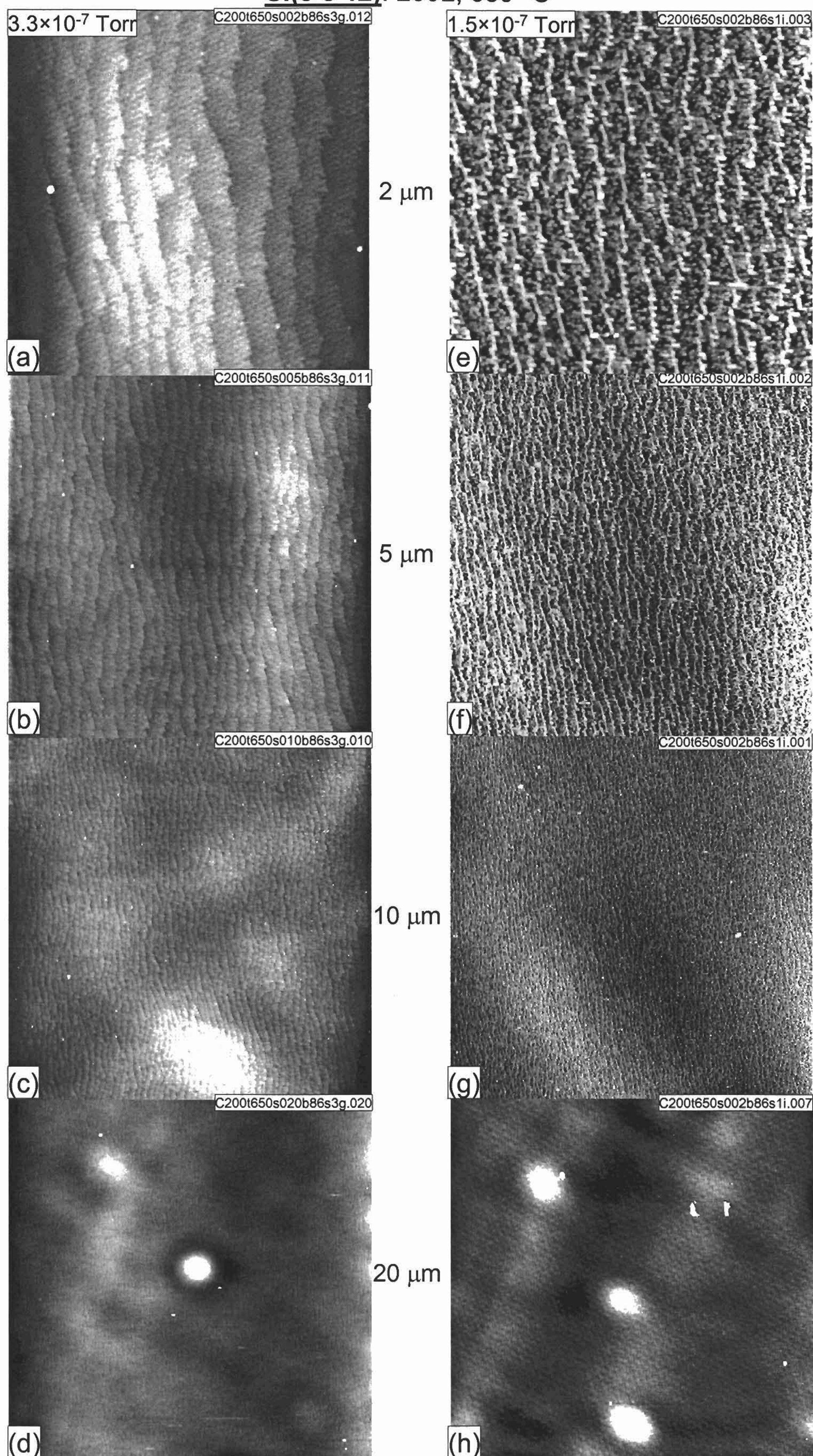

Si(5 5 12): 200L, 650 °C
3.3×10-7 Torr
C200t650s002b86s3g.012
1.5×10-7 Torr
C200t650s002b86s1i.003
2 µm
(a)
(e)
C200t650s005b86s3g.011
C200t650s002b86s1i.002
5 µm
(b)
(f)
C200t650s010b86s3g.010
C200t650s002b86s1i.001
10 µm
(c)
(g)
C200t650s020b86s3g.020
C200t650s002b86s1i.007
20 µm
(d)
(h)

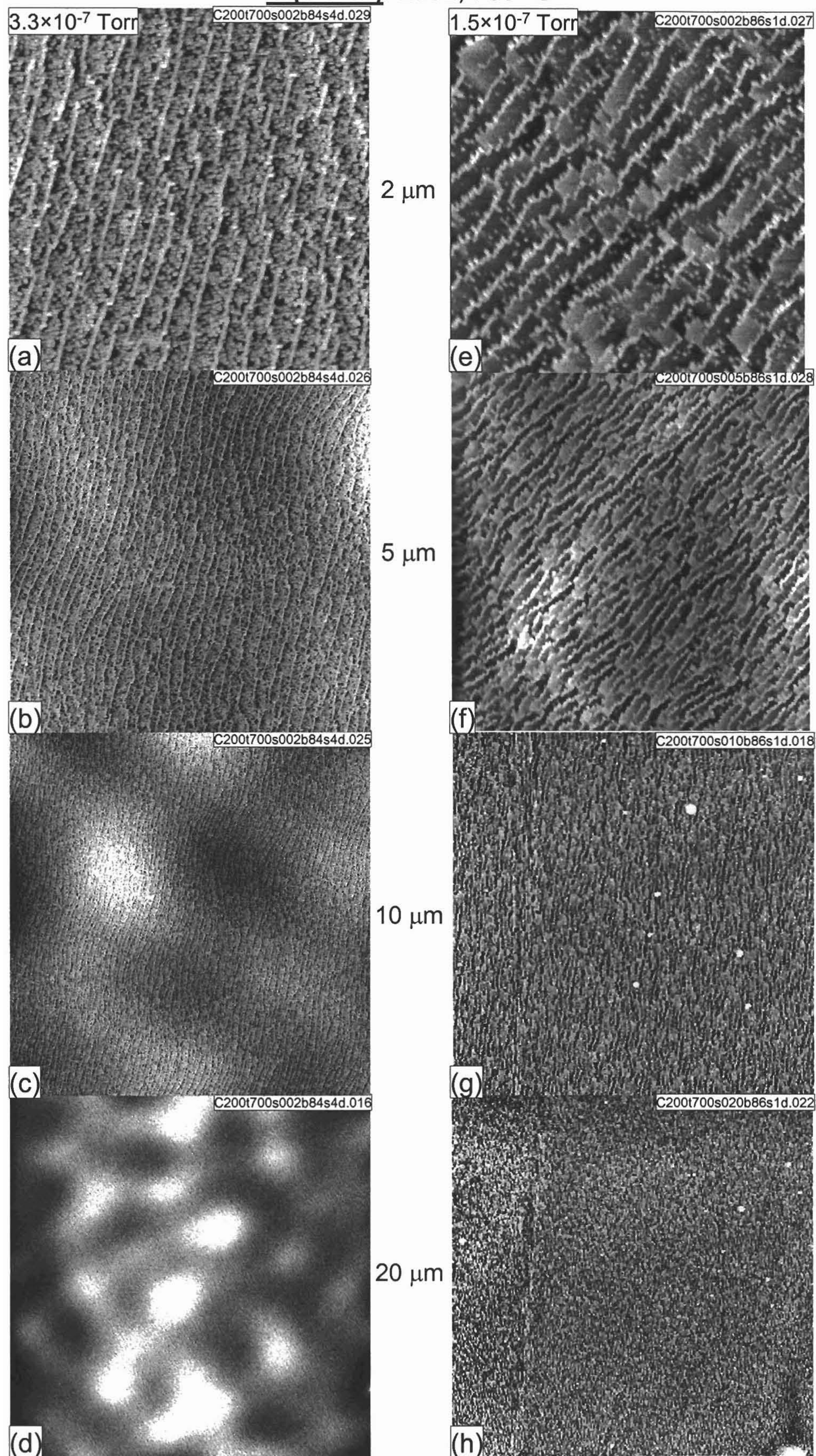

Appendix

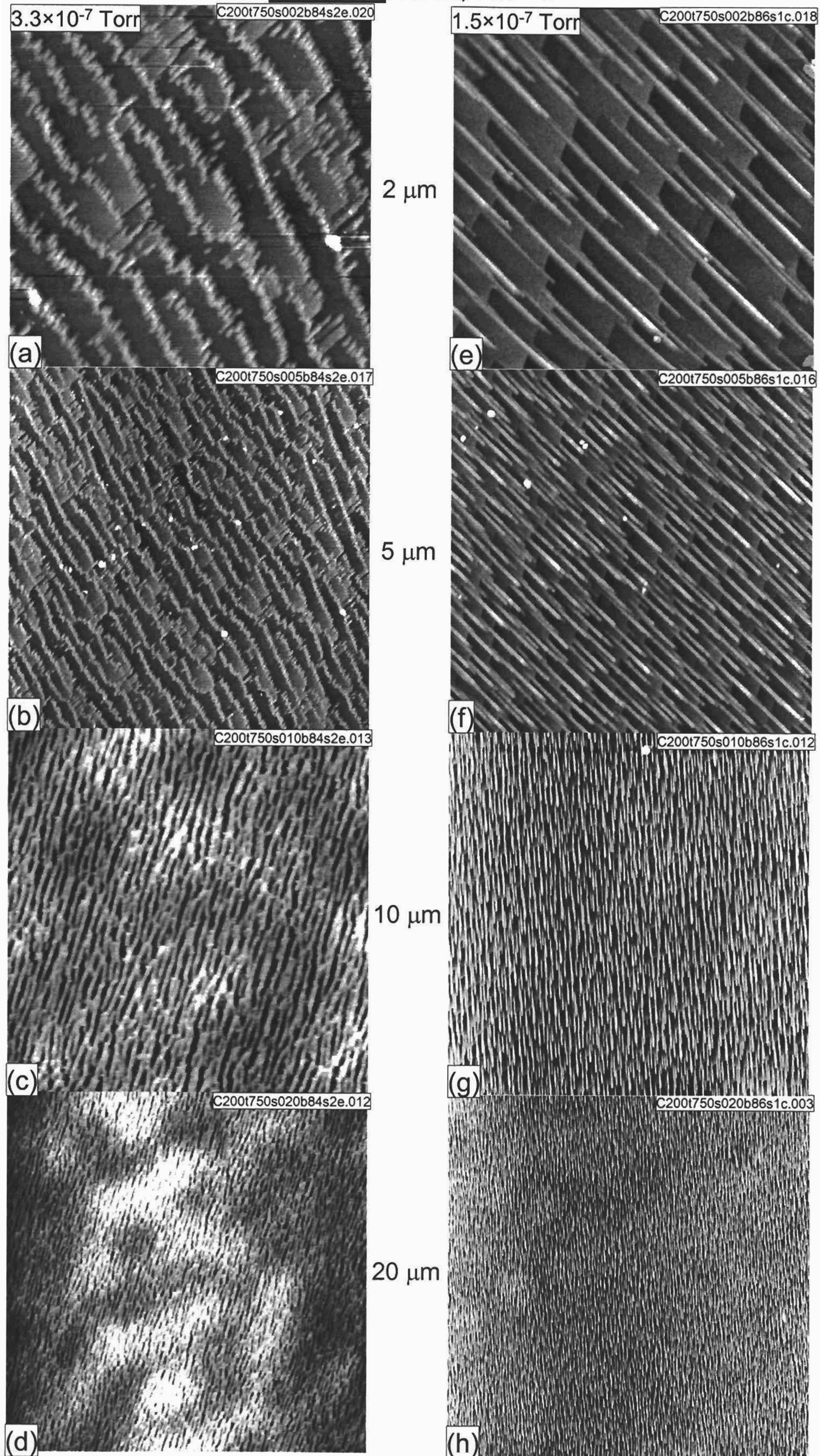
Si(5 5 12): 200L, 750 °C
3.3×10-7 Torr
C200t750s002b84s2e.020
1.5×10-7 Torr
C200t750s002b86s1c.018
2 μm
(a)
(e)
C200t750s005b84s2e.017
C200t750s005b86s1c.016
5 μm
(b)
(f)
C200t750s010b84s2e.013
C200t750s010b86s1c.012
10 μm
(c)
(g)
C200t750s020b84s2e.012
C200t750s020b86s1c.003
20 μm
(d)
(h)

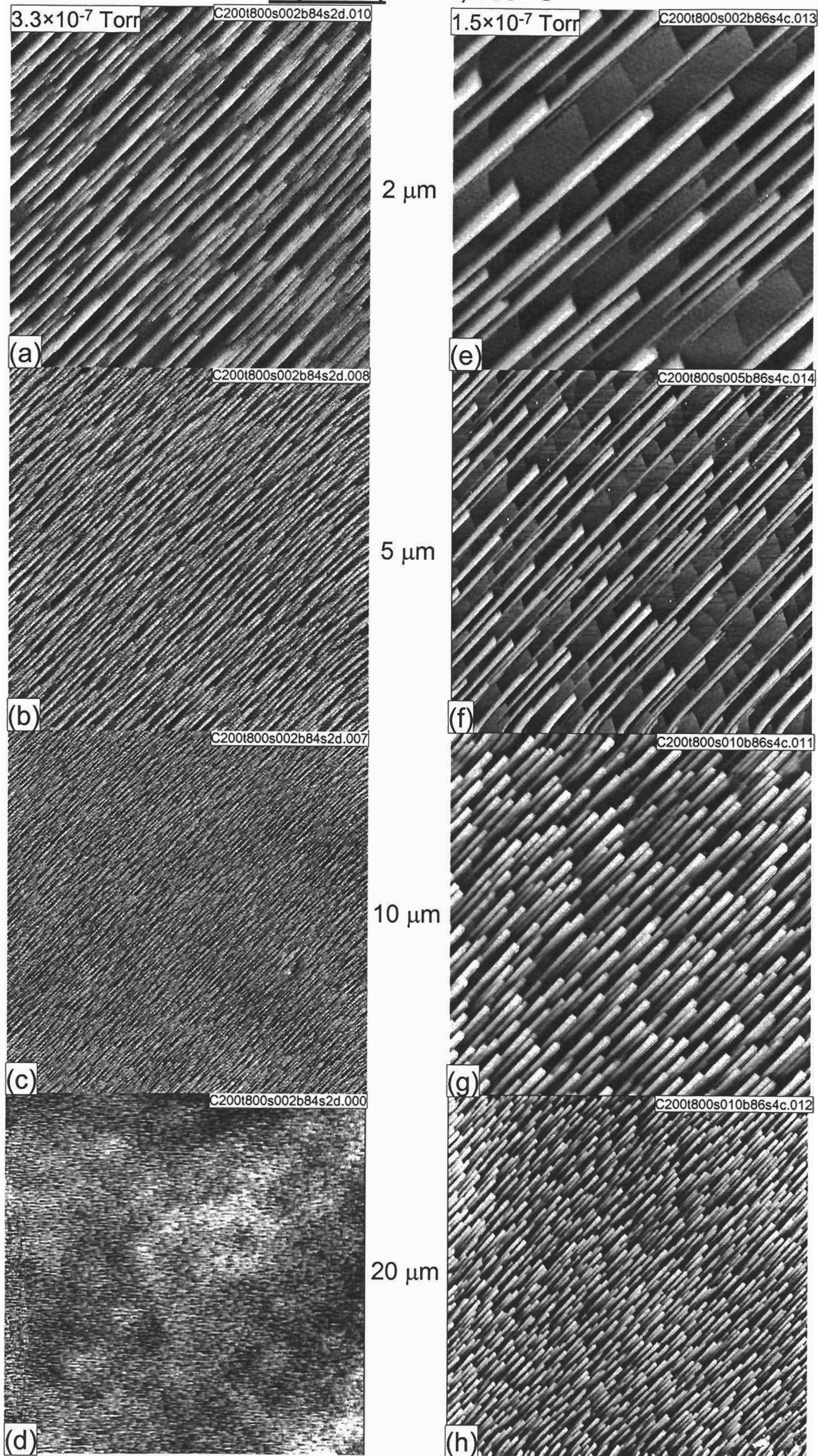

Si(5 5 12): 200L, 800 °C
3.3×10-7 Torr
C200t800s002b84s2d.010
1.5×10-7 Torr
C200t800s002b86s4c.013
2 μm
(a)
(e)
C200t800s002b84s2d.008
C200t800s005b86s4c.014
5 μm
(b)
(f)
C200t800s002b84s2d.007
C200t800s010b86s4c.011
10 μm
(c)
(g)
C200t800s002b84s2d.000
C200t800s010b86s4c.012
20 μm
(d)
(h)